Satellite Observations of the Wind Jets off the Pacific Coast of Central America. Part I: Case Studies and Statistical Characteristics

DUDLEY B. CHELTON, MICHAEL H. FREILICH, AND STEVEN K. ESBENSEN

College of Oceanic and Atmospheric Sciences, Oregon State University, Corvallis, Oregon

(Manuscript received 15 September 1998, in final form 12 July 1999)

ABSTRACT

Measurements of near-surface winds by the NASA scatterometer (NSCAT) from October 1996 through June 1997 are analyzed to investigate the three major wind jets along the Pacific coast of Central America that blow over the Gulfs of Tehuantepec, Papagayo, and Panama. Each jet is easily identifiable as locally intense offshore winds in the lee of low-elevation gaps through the Sierra Madre mountain range. The jets have relatively narrow cross-stream width but often extend several hundred kilometers or more into the Pacific. The Tehuantepec and Papagayo jets sometimes merge with the northeast trade winds of the Pacific.

The Tehuantepec jet was highly energetic with characteristic timescales of about 2 days. Events were triggered by high pressures associated with cold surges into the Gulf of Mexico that originated over the Great Plains of North America. The Papagayo and Panama jets were much more persistent than the Tehuantepec jets. The winds at both of these lower-latitude locations exhibited a strong seasonal variation with almost exclusively offshore flow from late November 1996 through late May 1997 and periods of onshore flow in October and November during the late stages of the 1996 Central American monsoon season. Superimposed on this low-frequency seasonal variation were events with characteristic timescales of a few days.

Based on NSCAT data, the spatial and temporal evolution of major wind events is described in detail for three representative case studies. In December 1996, the jets developed sequentially from north to south, consistent with the notion that wind events in the two lower-latitude jets are associated with cold-air outbreaks that trigger the Tehuantepec jet a day or so earlier. In November 1996 and March 1997, the Papagayo and Panama jets were strongly influenced by tropical phenomena that had little apparent association with the Tehuantepec jet. These latter two case studies, together with the distinction between the statistical characteristics of the three jets, suggest that the Papagayo and Panama jets are predominantly controlled by a mechanism that is very different from the across-gap pressure gradients associated with high pressure systems of midlatitude origin that control the Tehuantepec jet.

1. Introduction

The Sierra Madre mountain range that extends the full length of Mexico and Central America forms a nearly complete barrier between two very different low-level air masses. The warm air in the eastern tropical Pacific is characterized by relatively low sea level pressure (SLP). Surges of cold air of midlatitude origin that move southward over the Gulf of Mexico during the fall, winter, and spring result in SLP that often exceeds the eastern tropical Pacific SLP by 5 hPa or more. The existence of three low-elevation gaps through the mountains (elevations below 300 m, see Fig. 1), in combination with this large difference in SLP across the Central American isthmus,[1] create unique meteorological conditions. The cross-isthmus pressure gradients can generate intense wind jets[2] that blow through all three gaps and into the Pacific over the Gulfs of Tehuantepec, Papagayo,[3] and Panama. Since the Sierra Madre also form a barrier to the Caribbean trade winds at altitudes below the

Corresponding author address: Dudley B. Chelton, College of Oceanic and Atmospheric Sciences, Oregon State University, 104 Ocean Admin Building, Corvallis, OR 97331-5503.
E-mail: chelton@oce.orst.edu

[1] For the purposes of discussion in this paper, the Isthmus of Tehuantepec is considered to be in Central America, although Mexico is not strictly part of Central America.

[2] The term ''jet'' as used in this study is defined subjectively to be a localized region of strong offshore winds in the lee of the three low-elevation gaps through the Sierra Madre. Jets with core speeds in excess of 10 m s^{-1} are arbitrarily distinguished here as ''strong'' events.

[3] The western end of the gap formed by the Nicaraguan lake district spans a broad region extending from the Gulf of Papagayo at 10.5°N to the Gulf of Fonseca at 13°N (see Fig. 1). It is shown in Fig. 11a below that the mean location of the core of the jet is at about 11.5°N. Although this is north of the Gulf of Papagayo, this jet is referred to here in the traditional manner as the Papagayo jet.

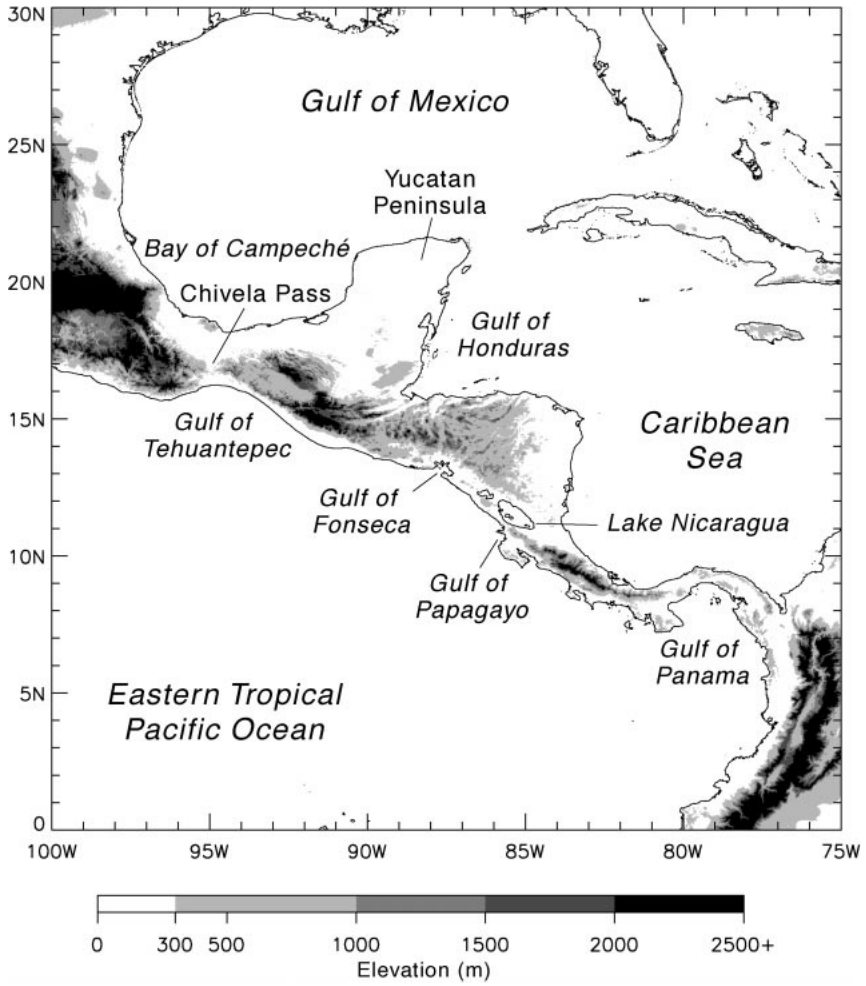

FIG. 1. Map of the topography and geographical locations referred to in this paper. The gray-shade key at the bottom of the plot indicates the elevation ranges of the Sierra Madre mountain range.

~750-m elevations of the mountains in Nicaragua, Costa Rica, and Panama, wind jets over the Pacific can also be created by the funneling of trade winds through the Papagayo and Panama gaps.

Telltale signs of the existence of the three wind jets are the three plumes of cold water that often extend several hundred kilometers or more into the Pacific in the lee of the three gaps. These cold-water plumes are created by intense vertical mixing of the ocean that entrains the cold water and nutrients from the deep water into the surface layer (McCreary et al. 1989; Barton et al. 1993; Trasviña et al. 1995). This mixing has a profound effect on the upper-ocean temperature, sometimes decreasing the sea surface temperature (SST) by 8°C in a period of less than 24 h after the onset of a major wind event (e.g., Stumpf 1975; Legeckis 1988; Clarke 1988; Barton et al. 1993; Trasviña et al. 1995). The injection of nutrients into the euphotic zone dramatically influences the distributions of phytoplankton (Fiedler 1994; Lluch-Cota et al. 1997) and zooplankton (Färber-Lorda et al. 1994), especially in the Gulf of Tehuantepec.

It is well established that the Tehuantepec jet is triggered by cold-air outbreaks that originate over the Great Plains of North America (Hurd 1929; Parmenter 1970; Schultz et al. 1997; Steenburgh et al. 1998). From a comprehensive analysis of historical data, Schultz et al. (1998) showed that the equatorward penetration of cold fronts varies from event to event. Those cold fronts that reach the southwestern Caribbean create relatively high surface pressure on the upwind sides of the Papagayo and Panama gaps, thereby generating gap throughflows. It is widely presumed that this is the primary mechanism for generation of the Papagayo and Panama jets. The basis for this view that the Papagayo and Panama jets are linked to cold-air outbreaks that trigger the Tehuantepec jet a day or so earlier is largely anecdotal since published observational and modeling studies have overwhelmingly emphasized the Tehuantepec jet.

Sequential north-to-south triggering of the three jets by high-pressure systems of midlatitude origin that move southeastward across the Inter-American Seas[4] was apparently first suggested by Hurd (1929). In what appears to be the only published confirmation of sequential triggering of the three jets, Schultz et al. (1997) documented a case study from March 1993 during which the Papagayo and Panama jets appeared about 12 h after the onset of a strong Tehuantepec jet in association with a major cold surge that penetrated into the southwest Caribbean.

Although the north-to-south triggering of the three jets during major cold-air outbreaks is an appealingly simple explanation for the generation of Papagayo and Panama wind jets, statistical studies have not yet been conducted to assess the generality of the link of these jets to high-pressure systems of midlatitude origin. Observational information about the Papagayo jet is especially limited. Because of the sparse distribution of oceanic wind observations in this region, there have been no detailed studies of the Papagayo jet. An analysis of two weeks of satellite observations of SST by Legeckis (1988) raises questions about whether the Papagayo and Panama jets are linked to Tehuantepec wind events. From the persistence of cold-water plumes downwind of the Papagayo and Panama gaps in a sequence of satellite observations of SST during March 1985, Legeckis (1988) inferred that the Papagayo and Panama jets were blowing persistently during a 2-week period when the Tehuantepec jet was relatively weak. He therefore concluded that the Papagayo and Panama jets are not always synchronous with the Tehuantepec jet.

Winds in the Panama region have been studied in greater detail. The opening of the Panama Canal in 1914 motivated two major investigations of the winds near the Isthmus of Panama. Frankenfield (1917) and Chapel (1927) both concluded that wind variability in this region was associated primarily with trade wind variability. They distinguished the normal trade wind–driven Panama winds from infrequent ''northers'' associated with high pressure systems of midlatitude origin that affected the Panama winds only about once per year.

The historical analyses of Panama winds by Frankenfield (1917) and Chapel (1927) and the SST observations in the vicinities of the Papagayo and Panama jets by Legeckis (1988) thus suggest that some mechanism besides cold-air outbreaks must be responsible for the generation of the Papagayo and Panama jets during at least some events. Observational studies of the generation mechanisms for the three Central American jets have been limited by the sparse distribution of surface-wind observations throughout the eastern tropical Pacific. Historical in situ observations do not resolve the offshore structure and spatial extent of the three jets or the relationships between their temporal evolutions. The limited spatial coverage of in situ observations of surface winds can be alleviated by a satellite scatterometer, which is a spaceborne radar designed to measure vector winds over the ocean. Wind speed and direction are inferred from the roughness of the sea surface (see section 2 and section a of the appendix). The model function for estimating vector winds from scatterometer measurements of radar backscatter is calibrated to neutral-stability winds (Liu and Tang 1996) at a reference height of 10 m above the sea surface.

In this study, measurements by the National Aeronautics and Space Administration (NASA) scatterometer (NSCAT) during the 9-month period from October 1996 through June 1997 are analyzed to investigate the surface wind fields in the eastern tropical Pacific. The objective is to characterize the statistics of the variability of each of the three jets during the 9-month NSCAT data record and to describe in detail the wind field evolution during representative time periods. As summarized in section 2 and described in more detail in the appendix, the NSCAT observations provide a description of the three Central American wind jets with unprecedented spatial and temporal coverage. The diversity of the relationships between the jets is illustrated from three case studies in section 3. The statistical characteristics of the three jets are summarized in section 4. One of the primary conclusions from this analysis is that each of the jets was distinct in character during the NSCAT mission. The statistical relationships between variations in the intensities of the three jets and dynamical balances within the jets are quantitatively investigated in a companion paper (Chelton et al. 2000).

2. Data description

The wind observations analyzed in this study were acquired by NSCAT, a spaceborne microwave radar instrument designed specifically to measure near-surface wind velocity (both speed and direction) over the oceans under near all-weather conditions. Launched onboard the Japanese Advanced Earth Observing Satellite (ADEOS) in August 1996, NSCAT observed the wind field over the global ocean nearly continuously from mid-September 1996 until the catastrophic failure of the spacecraft's solar panel abruptly ended the ADEOS mission on 30 June 1997. The principles of scatterometry and details of the NSCAT instrument design and data processing are presented in Naderi et al. (1991) and the references therein. Brief overviews of essential instrument and data characteristics are presented below; more detailed summaries are given in the appendix.

NSCAT used eight antennas (four on each side of the spacecraft) to transmit pulses of 14-GHz microwave radiation and measure the energy backscattered from the

[4] By definition, the Inter-American Seas comprise the Gulf of Mexico, the Caribbean Sea, and the Straits of Florida.

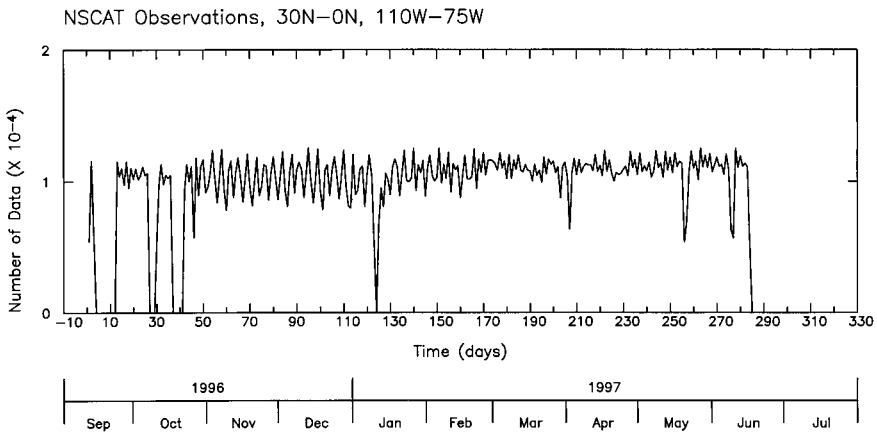

FIG. 2. Time series of the daily total number of NSCAT samples of 10-m winds within the latitude range from the equator to 30°N and the longitude range from 110° to 75°W.

sea surface. The normalized radar cross section (σ_0) was determined for footprints with typical dimensions of 6 km $\times$ 25 km across two 600-km swaths separated by a 329-km gap centered on the satellite ground track. The returned signal backscatters primarily from centimetric-scale ocean roughness elements whose amplitudes and orientations are highly correlated with wind speed and direction. Vector winds with ~25-km spatial resolution were estimated within each 600-km swath by combining collocated, near-simultaneous σ_0 measurements obtained from the four different antennas on the corresponding side of the spacecraft. The NSCAT winds analyzed here were calculated using the NSCAT-1 model function (Wentz and Smith 1999; Freilich and Dunbar 1999, unpublished manuscript) and a maximum likelihood retrieval algorithm (Naderi et al. 1991). The wind retrieval processing resulted in typically four possible vector wind solutions (''ambiguities'') at each location; a circular median filter algorithm was used to select a unique vector wind solution (Naderi et al. 1991, and references therein).

Freilich and Dunbar (1999) and Freilich and Vanhoff (2000, submitted to *J. Atmos. Oceanic Technol.*) have quantified the accuracy of the NSCAT-1 winds from comparisons with buoy anemometer measurements at 30 midlatitude locations during the 9-month NSCAT data record. They concluded that the NSCAT wind speeds had a relative speed bias of -0.3 m s^{-1} (NSCAT speeds lower than buoy speeds) and a root-mean-square (rms) difference of 1.2 m s^{-1}. Directional differences of more than 90° between an NSCAT measurement and a buoy observation are probably indicative of large errors in the median filter ambiguity removal algorithm applied to the NSCAT data (see section b of the appendix). For wind speeds exceeding 6 m s^{-1}, this occurred for only 3% of the buoy collocations. When these gross ambiguity removal errors were excluded, the mean directional difference was 8° (NSCAT clockwise relative to the buoy winds) and the standard deviation of the differences was 17° for wind speeds from 3 to 20 m s^{-1}. A validation based only on NSCAT comparisons with buoys in the Gulf of Mexico and the northeastern tropical Pacific regions of interest in this study yields similar differences between the NSCAT and buoy estimates of wind speed and direction (see section c of the appendix).

It is important to note that part of the rms differences between the NSCAT and buoy winds is attributable to errors in the buoy measurements. Independent assessments of buoy winds by Gilhousen (1987), Beardsley et al. (1997), and Freilich and Vanhoff (2000, submitted to *J. Atmos. Oceanic Technol.*) conclude that the uncertainties of buoy wind speeds and directions are about 0.8 m s^{-1} and 10°, respectively. The root sum of squares partitioning of the rms differences between NSCAT and buoy winds thus leads to the conclusion that the NSCAT measurement accuracy is very similar to that of the buoy measurements.

From these buoy comparisons and from the maps and time series of the NSCAT winds presented in sections 3 and 4, we believe that the NSCAT vector wind measurements are reliable for investigating the Central American wind jets that are the focus of this study. The NSCAT dataset provides a far more complete spatial sampling of these jets than has heretofore been available.

A time history of the daily total number of NSCAT observations in the study area from the equator to 30°N and from 110° to 75°W is shown in Fig. 2. With the exception of two periods during October 1996 when NSCAT was powered off during startup of other instruments on ADEOS and one other data gap in January 1997, NSCAT acquired approximately 10 000 surface wind observations per day in this region. Although the NSCAT dataset far exceeds the spatial and temporal coverage available from in situ measurements, there are two types of sampling errors that exist in gridded wind fields constructed from NSCAT data. The first arises

from the fact that the combined area of the four σ_0 measurements used to retrieve each vector wind estimate is approximately (25 km)^2 (see appendix). Spatial variations of wind speed and direction with scales shorter than ~25 km are sampled differently by the four antennas. Furthermore, the centroids of the backscatter measurements are not perfectly collocated, leading to a somewhat smoothed wind velocity estimate in regions where horizontal gradients of the wind field are large over scales shorter than ~25 km.

A more problematic sampling error results from the finite measurement swaths and the satellite orbital characteristics. The NSCAT measurement pattern near Central America is illustrated in Fig. 3 by examples showing the NSCAT observations during two consecutive 8-h periods. (A 48-h composite map centered on the same time period is shown in Fig. 9b below.) The occasional narrow diagonal gaps across the NSCAT measurement swaths are calibration cycles. The other occasional missing wind vectors are the result of poorly collocated backscatter measurements from the four antennas and inaccurate σ_0 measurements that were detected, flagged, and eliminated in the course of the ground-based data processing.

The time- and space scales that can be resolved in gridded wind fields constructed from NSCAT data remain subjects of investigation. To obtain relatively complete spatial coverage, the wind maps analyzed in section 3 were constructed as simple 2-day composite averages over 1° × 1° areas. Since the Tehuantepec jet often evolves very rapidly (sometimes developing over a period of less than half a day; see Schultz et al. 1997), the limitations of the 2-day averaging must be kept in mind. The NSCAT data obviously cannot resolve the detailed time evolution of rapidly evolving events. Despite this limitation, the spatial coverage of the NSCAT observations yields unprecedented information about the spatial structures of the jets. The NSCAT data also provide important new insight into the relationships between the three jets and the surrounding wind field in the Inter-American Seas and the eastern tropical Pacific.

Over the latitudes of interest in this study, the NSCAT sampling yielded a mean revisit time of 23.5 h between measurements at any given location.[5] To improve the temporal resolution for the statistical analyses in section 4, the NSCAT measurements were composite averaged over 1-day time intervals and 1° × 1° areas. This shorter averaging period typically resulted in no temporal smoothing at all. When ascending and descending measurement swaths intersected within a day, the composites consisted of the average of measurements at the same location during the two orbits. The 1-day composite averaging resulted in missing data values in the daily time series at any particular location (see Figs. 10 and 13 below).

[5] The sampling limitations of NSCAT will be substantially reduced by the next-generation QuikSCAT scatterometer that launched in June 1999 and the technologically identical Sea-Winds scatterometer scheduled for launch in November 2001. The scanning design of these scatterometers eliminates the nadir gap in the NSCAT sampling, thus significantly improving the spatial coverage. The mean revisit time for a single scanning scatterometer is 19 h at 15° lat. The revisit time would be further reduced to 9 h for a tandem QuikSCAT and SeaWinds scanning scatterometer mission.

3. Case study examples of Central American wind jets

The diversity of mechanisms that affect the prominent wind jets along the Pacific coast of Central America is illustrated in this section from three representative time periods using NSCAT observations and the National Centers for Environmental Prediction (NCEP) reanalyzed fields of SLP and 10-m winds available on a 2.5° × 2.5° grid (Kalnay et al. 1996). In the conventional view summarized in the introduction, surges of Papagayo and Panama wind jets are triggered sequentially following major Tehuantepec jets in response to high pressure systems that originate over the Great Plains of North America and penetrate as far south as the southern Caribbean Sea. The first case study considered here evolves in accord with this scenario. The other two case studies show examples in which the Papagayo and Panama jets are controlled by tropical phenomena that had little or no influence on the Tehuantepec jet.

The three case studies summarized here are illustrated from selected 2-day average maps of the NSCAT wind observations. The complete evolution of each wind event can be viewed from the animation of the full 9-month NSCAT data record on the following web site: http://www.oce.orst.edu/po/research/windjets/movie.html.

a. December 1996

The first case study spans a 10-day period in December 1996 during which a strong cold surge through the Tehuantepec gap was followed 1 day later by the development of a Papagayo jet and 2 days later by the development of a Panama jet. This sequential triggering of the three gap outflows closely follows the conventional view of the north-to-south development of the wind jets along the Pacific coast of Central America first suggested by Hurd (1929) and recently documented in detail by Schultz et al. (1997).

This case study began on 16 December when a weak anticyclone of midlatitude origin generated a southward surge in the far western Gulf of Mexico. These northerly winds along the eastern slope of the Sierra Madre subsequently abated as the midlatitude system continued to move eastward. On 17 December, there was no evidence in NCEP reanalyses or the NSCAT data of any significant flow through the Tehuantepec gap (Figs. 4a and 5a). Gap outflow over the Gulf of Papagayo was moderate and the winds were calm over the Gulf of Panama. (Note that the high SLP over the spine of the Sierra

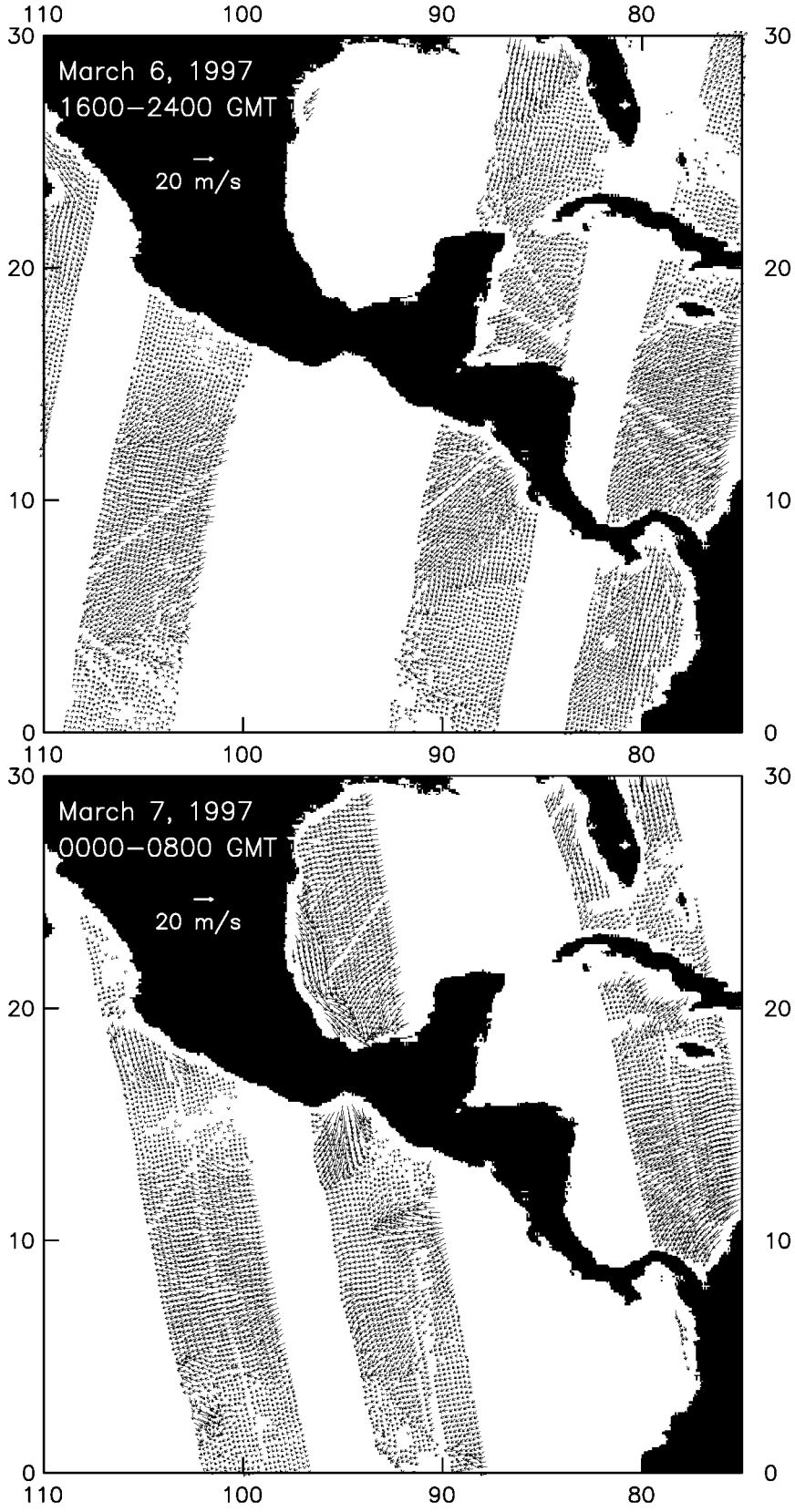

FIG. 3. NSCAT observations of 10-m vector winds during the 8-h periods preceding and following 0000 GMT 7 Mar 1997.

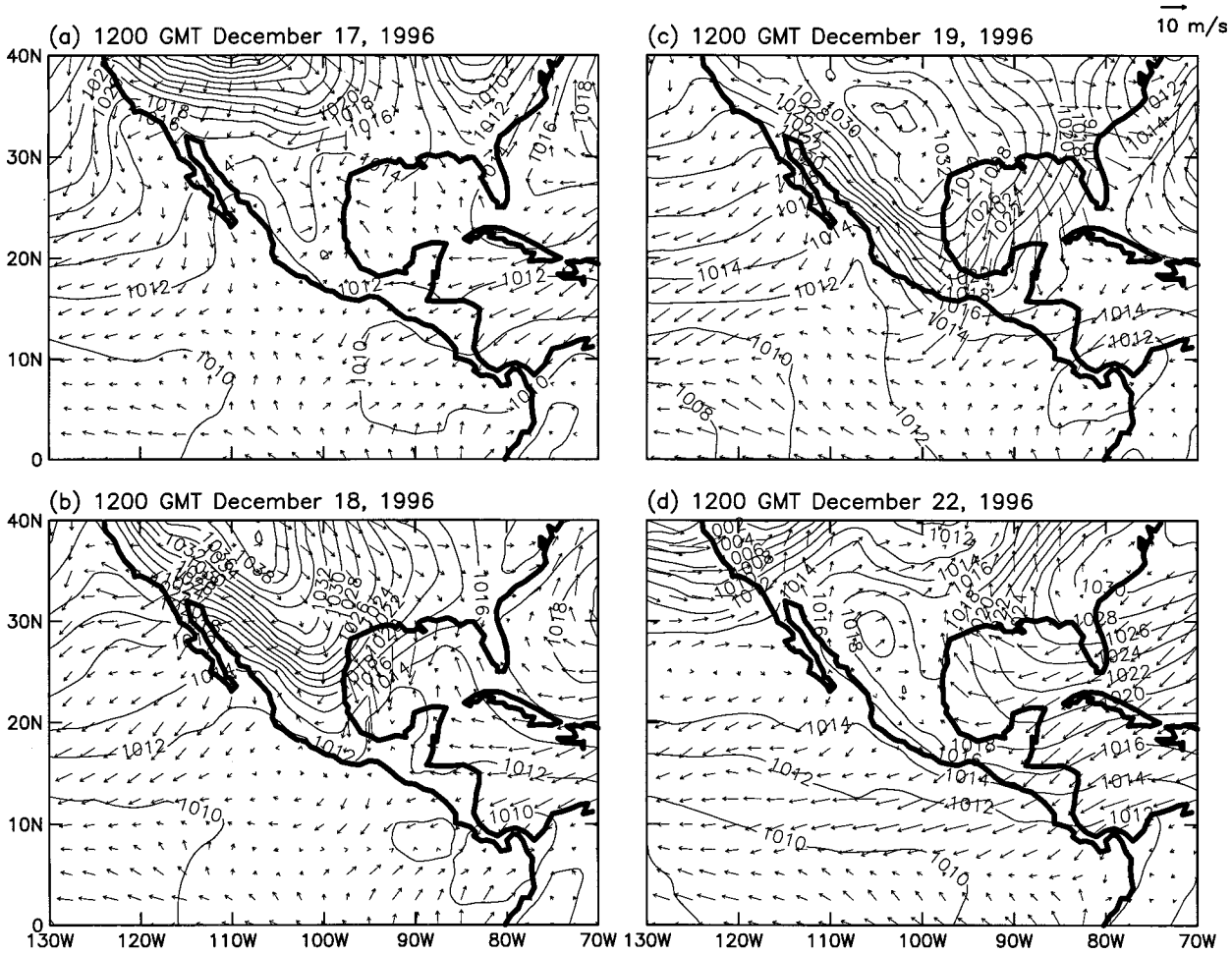

FIG. 4. Sea level pressure and 10-m winds from the 2.5°-gridded NCEP reanalyses for the selected times indicated during the Dec 1996 case study.

Madre may be due to problems in reducing surface pressure to sea level in regions of elevated terrain.)

Over the period 18–19 December, a strong midlatitude anticyclone generated a surge of northerly winds and associated increased SLP that moved southward along the eastern slope of the Sierra Madre and into the Bay of Campeché (Figs. 4b and 4c). A Tehuantepec jet developed rapidly on 19 December (Fig. 5b) in response to the large SLP increases in the southwestern Gulf of Mexico between 1800 GMT 18 December and 0600 GMT 19 December. Gap outflows over the Gulfs of Papagayo and Panama were weak at this time.

On 19 December, strong northerly winds developed over the entire Gulf of Mexico (Fig. 4c). During the next 24 h, these winds switched to easterlies in the western Gulf and northeasterlies in the eastern Gulf and the winds in the Bay of Campeché weakened (Fig. 5c). The details of this rapid evolution that cannot be resolved in 2-day composite averages of NSCAT data are not the primary concern here. The important point is that the strong jet that first appeared over the Gulf of Tehuantepec on 19 December persisted and spread more than 600 km southward on 20 December. Wind directions within the jet turned anticyclonically toward the west. A Papagayo jet began to develop near the coast but winds over the Gulf of Panama remained weak (Fig. 5c).

During 21–23 December, the trade winds increased throughout the Caribbean Sea (Figs. 4d, 5c, and 5d). Northeasterly winds developed across a broad zonal band centered near 8°N in the Pacific. A Panama jet began to develop with limited areal extent on 21 December (not shown).

On 22 December, the surface anticyclone moved eastward across the Gulf of Mexico (Fig. 4d), weakening the cross-isthmus pressure gradient and causing a decrease in the intensity of the flow through Chivela Pass. By 24 December, winds over the Gulf of Tehuantepec had weakened but the Papagayo and Panama jets persisted, although with continued limited areal extent (Fig. 5d). The region of strong winds in the Gulf of Mexico

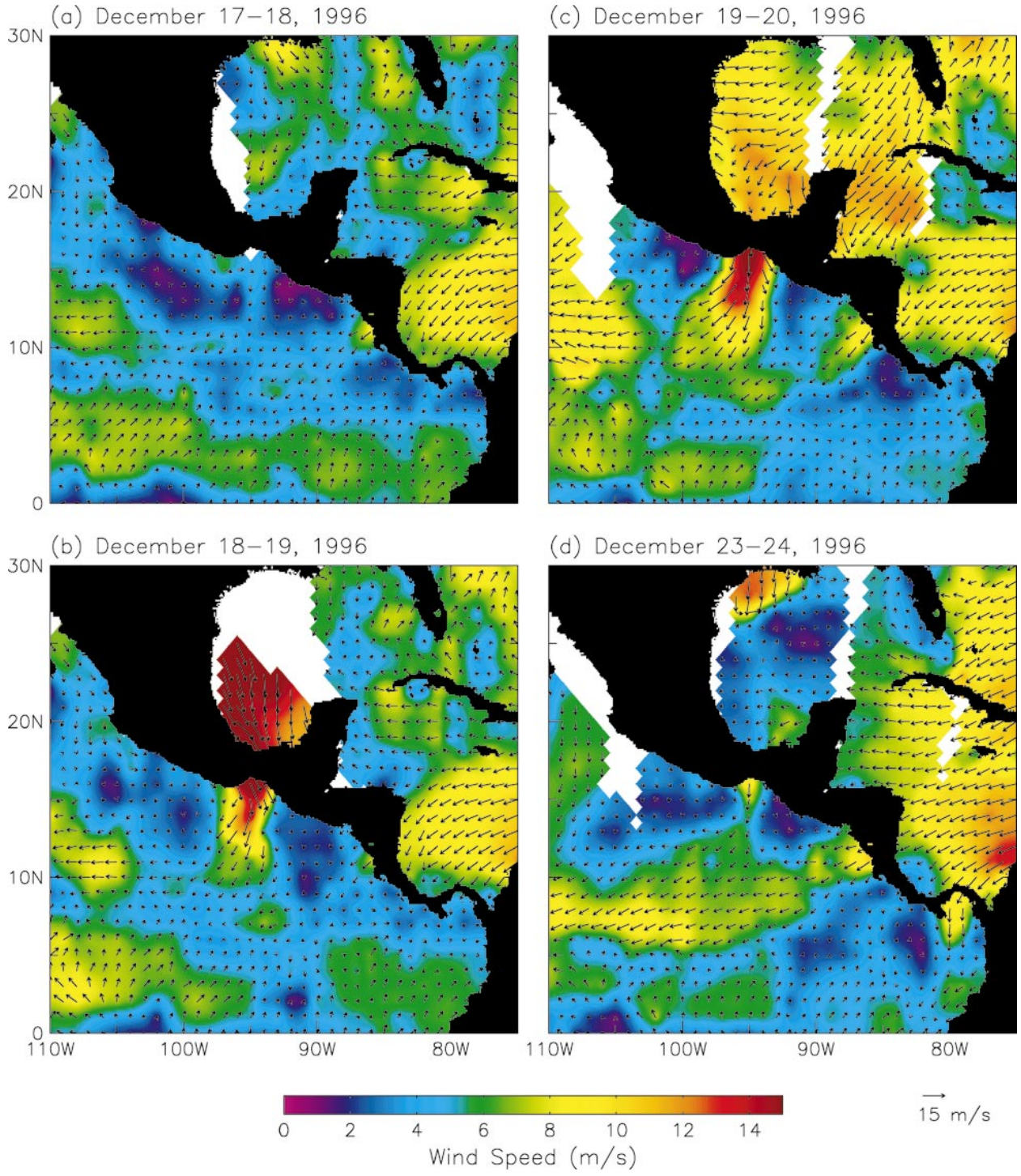

FIG. 5. Two-day composite averages of the wind field at 10 m over 1° × 1° areas from NSCAT data for the selected periods indicated during the Dec case study. The color table for the wind speed has been selected so that the transition from yellow to red occurs at 10 m s^{-1}, defined somewhat arbitrarily here to represent the transition from moderate to strong winds. The actual wind speed at any grid location can be inferred by comparison of the length of the vector at that location with the scale vector at the lower right corner of the plot. (An isolated example of an approximate 180° ambiguity removal error, see section b of the appendix, can be seen in the 18–19 Dec panel at 14°N, 94°W on the far eastern edge of the Tehuantepec jet.)

moved eastward into the western Atlantic and strong trade winds continued to blow in the Caribbean.

b. November 1996

The second case study spans a 2-week period in November 1996 during which a complex development of the three jets took place. The variability of the wind field in the region of interest was dominated by the occurrence of a major Tehuantepec event and the subsequent development of an unrelated tropical cyclone. At the beginning of the period, the three jets evolved in accord with the conventional view as in the December event summarized in section 3a. Toward the end of the period, however, onshore winds developed along most of the Pacific coast of Central America in association with the simultaneous development of tropical storm Marco in the western Caribbean (Bourassa et al. 1999) and a late-season surge in the eastern Pacific cross-equatorial flow. These tropical events also caused the Tehuantepec jet to turn cyclonically eastward over the Gulf of Tehuantepec. Two relatively weak Tehuantepec events that also occurred during this 2-week period had no apparent influence on the Papagayo and Panama jets.

The early stages of this case study began on 6 November when a surface low pressure system developed in the lee of the Rocky Mountains and moved northeastward across the United States. Similar to the December event in section 3a, an extensive area of high SLP developed rapidly behind this system. The southern edge of the high-pressure system moved southward over eastern Mexico and the western Gulf of Mexico. The high SLP reached the Gulf of Campeché on 8 November and an intense northerly jet developed rapidly over the Gulf of Tehuantepec (Figs. 6a, 7a, and 7b), turning anticyclonically westward and extending more than 1000 km into the Pacific. Offshore winds began to blow over the Gulf of Papagayo and strong northeasterly winds developed over the eastern Gulf of Mexico as the center of the high pressure system moved slowly eastward.

On 10 November, the areal extent of the strong winds downstream of the Tehuantepec gap decreased while the Papagayo jet intensified and a weak offshore flow began to develop over the Gulf of Panama (Fig. 7c). The maximum intensity of the Papagayo jet occurred near the Gulf of Fonseca, perhaps from flow through the canyon directly to the north (see Fig. 1).

On 12 November (not shown), the spatial extents of the Tehuantepec and Papagayo jets contracted toward the coast while the offshore Panama jet increased in strength, although the wind speeds were only about 6 m s^{-1}. A second Tehuantepec event occurred on 13 November in association with a moderate intensification of northerly winds in the far southwestern Gulf of Mexico (Figs. 6d and 7d). The wind speeds in this second event were somewhat lower and the spatial extent of the jet was much smaller than during the major Tehuantepec event that occurred 8–11 November. A strong north–south SLP gradient in the Gulf of Mexico was present throughout the period 12–16 November (Figs. 6d and 6e). As the center of the associated high pressure system over the United States moved eastward, however, SLP decreased over the southwestern Gulf of Mexico. The SLP difference across the Isthmus of Tehuantepec decreased significantly over the course of the day on 15 November the winds over the Gulf of Tehuantepec decreased in intensity and areal extent (Figs. 6e and 7e).

There was no evidence of triggering of Papagayo and Panama wind events after the second Tehuantepec event that occurred on 13 November. To the contrary, the winds in these two lower-latitude jets were under the influence of a synoptic-scale surface low-pressure system that began to develop on 13 November in the southern Caribbean Sea. A trough that initially extended to the northwest from northern Colombia intensified and moved to the northwest to become a closed cyclonic circulation center in the southwestern Caribbean on 14 November (Fig. 6d and 7d). Throughout the 2-week period of this case study, southerly flow covered most of a zonal band in the eastern Pacific between about 1°N and 6°N, extending at least as far west as 110°W (Figs. 7a–h). Coincident with the development of the Caribbean low-pressure system on 13 November, however, the southerly cross-equatorial flow increased from 95°W to the Gulf of Panama (Fig. 7d).

On 15 November, the Caribbean low altered the Papagayo and Panama jets. The effects of the Caribbean low have been described in detail by Bourassa et al. (1999). The winds reversed to become onshore over the Gulfs of Papagayo and Panama (Fig. 7e). Offshore winds appeared on the Caribbean side of the Papagayo gap and the far southeastern end of the Isthmus of Panama. The southwesterly surface flow across Panama recurved cyclonically around the eastern side of the surface low in the Caribbean, joining the trade wind flow entering the system in the northern Caribbean (Fig. 7e). Downstream from the Gulf of Tehuantepec in the Pacific, the jet began to turn cyclonically southeastward, connecting with the onshore flow entering the Papagayo gap (Fig. 7e). The Caribbean low-pressure system continued to intensify and became a tropical depression on 16 November.

During 17–22 November, the high SLPs over the eastern United States and northern Gulf of Mexico decreased (Figs. 6e–h) and the tropical low-pressure system in the western Caribbean intensified (Figs. 6e–h), apparently influencing the winds throughout the eastern tropical Pacific (Figs. 7e–h). The Papagayo and Panama winds continued to blow from the Pacific to the Caribbean on 17 November (Fig. 7f). Coincident with the onshore flow in the Papagayo region, the Tehuantepec jet decreased considerably and became northwesterly south of about 12°N. A localized region of high winds associated with the tropical depression is evident in the western Caribbean Sea at 14°N, 78°W in the 1°-averaged NSCAT wind field for 16–17 November (Fig. 7f). On

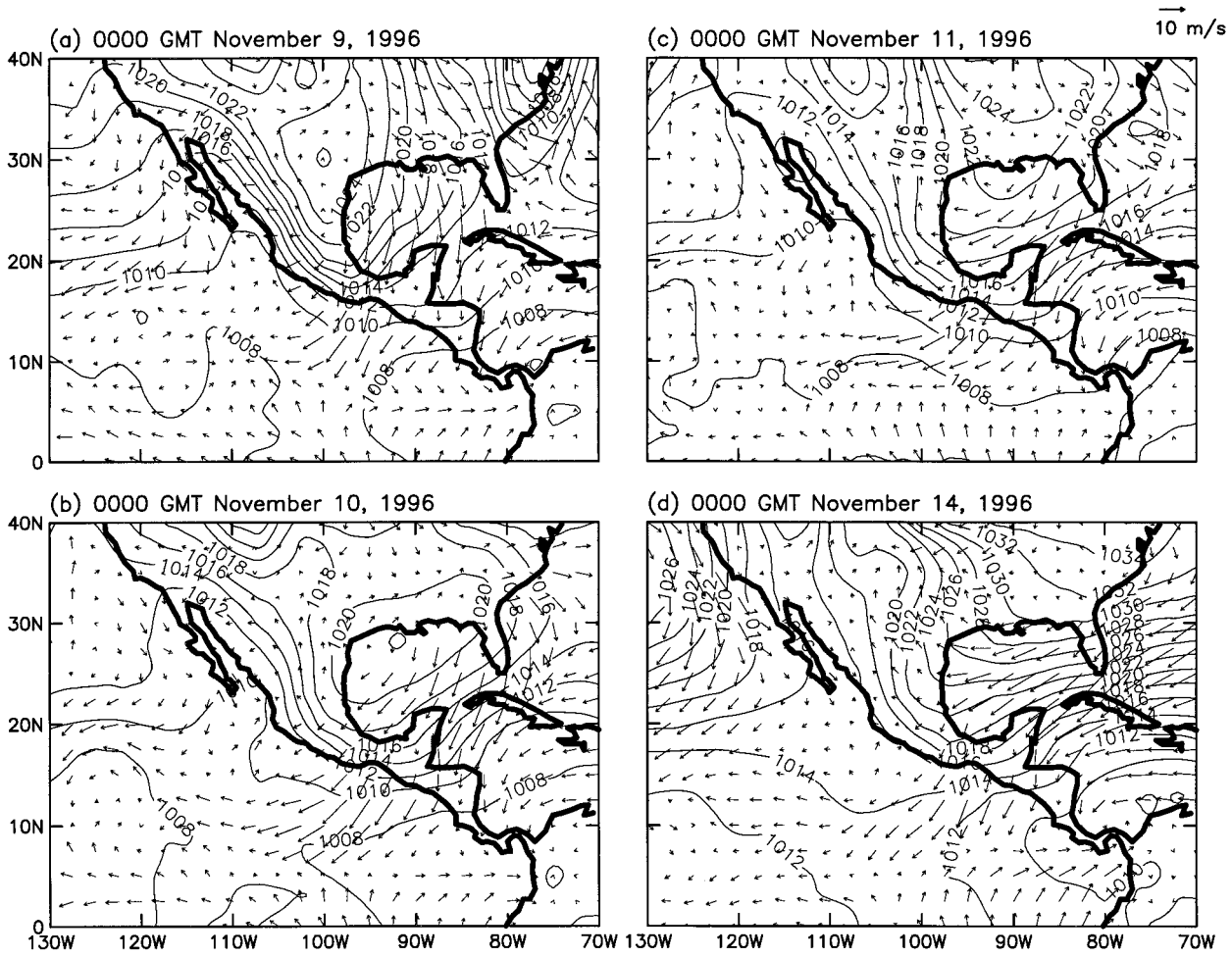

FIG. 6. Sea level pressure and 10-m winds from the 2.5°-gridded NCEP reanalyses for the selected times indicated during the November case study.

18 November, high SLP again arrived in the southwestern Gulf of Mexico and the flow through the Tehuantepec gap increased somewhat as another weak Tehuantepec wind event developed (Figs. 6g and 7g). The high pressure that triggered this Tehuantepec event did not penetrate far enough south to influence the Papagayo and Panama jets. The tropical depression in the Caribbean became tropical storm Marco on 19 November and briefly achieved hurricane status on 20 November. The intense winds associated with Marco are evident in Fig. 7h.

By 20 November, the SLP difference across the Isthmus of Tehuantepec decreased (Fig. 6h), ending the relatively minor Tehuantepec event (Fig. 7h). The Papagayo and Panama winds continued to blow onshore under the influence of the eastern Pacific trough and hurricane Marco in the Caribbean (Fig. 7h). During 20–22 November (not shown), Marco drifted slowly toward the east-northeast, causing decreases in the intensities of the Papagayo and Panama gap outflows into the Caribbean.

The association of week-long Papagayo and Panama gap outflows into the Caribbean with the formation of a cyclone in the western Caribbean during this case study is apparently typical of such wind conditions in these regions. Chapel (1927) noted that offshore winds into the Caribbean are restricted to occasional occurrences between September and November. From an 18-yr record of winds on the north side of the Isthmus of Panama during the period 1908–26, he identified 12 periods during which southerly winds persisted for more than 3 days. Ten of these cases coincided with the development of a cyclone in the western Caribbean.

c. March 1997

The third case study spans a 1-week period in early March 1997 during which the Caribbean trade winds exerted a persistent, strong influence on the Papagayo and Panama jets but had no apparent effect on the Tehuantepec jet. In association with strong Caribbean trade winds, the Papagayo and Panama jets were blowing in-

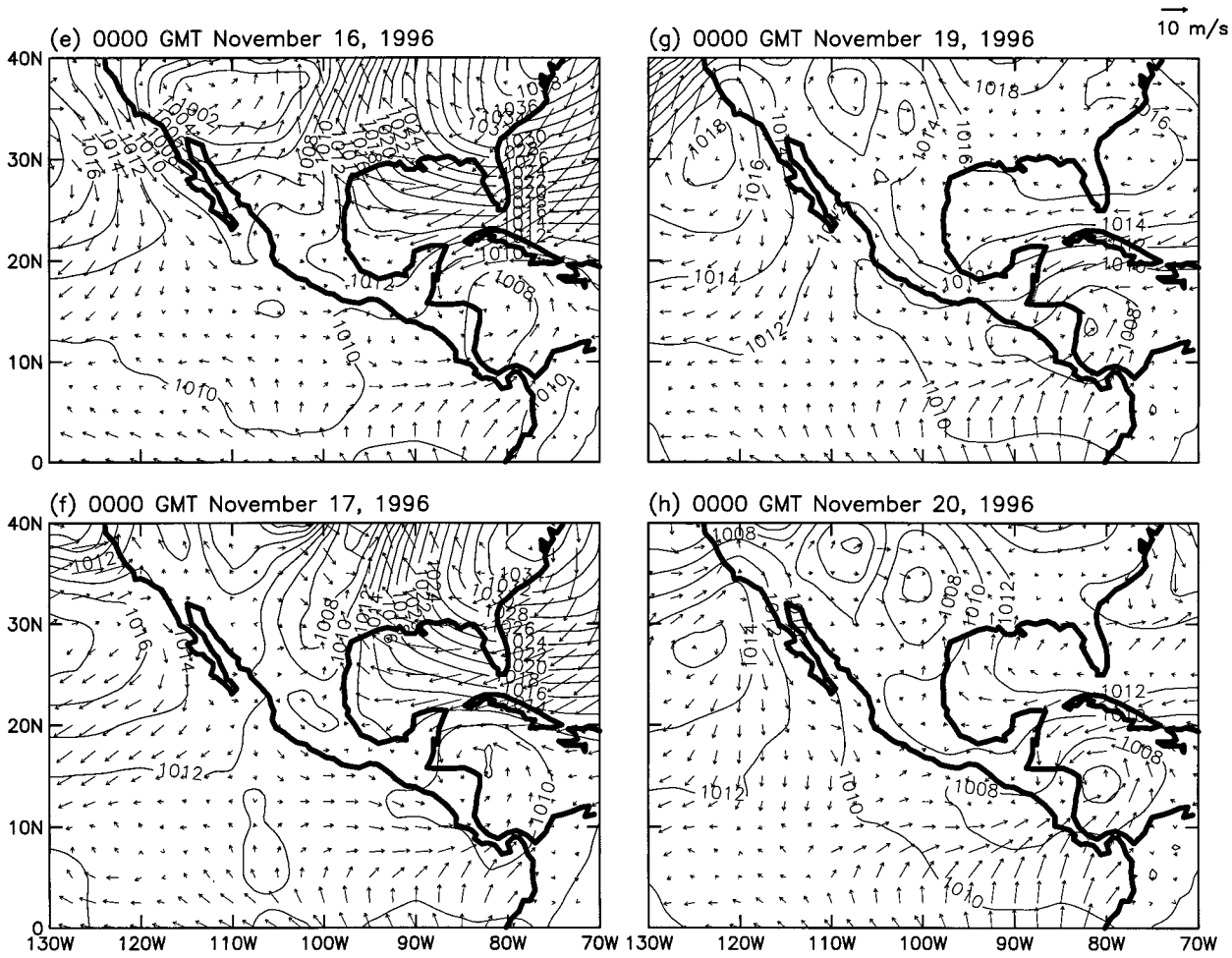

FIG. 6. (*Continued*)

tensely for more than 2 weeks prior to the onset of a transient Tehuantepec wind event. The Papagayo and Panama winds in this case study continued to blow after the Tehuantepec winds abated.

Prior to the 4 March beginning of this case study, moderate offshore winds were well established over the Gulfs of Papagayo and Panama, evidently in association with strong northeasterly winds over most of the Caribbean Sea. It is evident from the time series in Figs. 10 and 13 below that a strong offshore jet had been blowing over the Gulf of Papagayo for more than a month and the Panama jet had been blowing offshore for about 2 weeks. Over the first few days of March, an SLP trough moved eastward across the southern United States (Fig. 8a). During this same period, the Papagayo and Panama jets both increased in areal extent but the winds remained light over the Gulf of Tehuantepec (Fig. 9a). As in the case studies described in sections 3a and 3b (see also Colle and Mass 1995; Schultz et al. 1998), high SLP developed behind the low-pressure system and the winds in the Gulf of Mexico shifted from southeasterly to northeasterly as the trough passed (Figs. 8a, 8b, 9a, and 9b). The trade winds over the Caribbean Sea remained strong throughout this period.

By 6 March, northerly winds had surged into southeastern Mexico and the western Gulf of Mexico (Fig. 9b). The accompanying high SLP in the Bay of Campeché (Fig. 8b) caused the winds to increase dramatically over the Gulf of Tehuantepec. The Tehuantepec jet curved anticyclonically toward the west and extended far into the Pacific (Fig. 9b), merging with the trade winds that had previously been linked to the Papagayo jet (Fig. 9a). Strong Caribbean trade winds continued to blow but the Panama jet weakened somewhat.

During 7–10 March, a succession of low and high pressure systems moved across the southwestern United States into the Midwest. These SLP variations did not extend far enough south to drive winds through Chivela Pass (see, e.g., Fig. 8c). The winds over the Gulf of Tehuantepec rapidly decreased on 10 March (Fig. 9c). The Caribbean trade winds remained strong throughout the period and the Papagayo and Panama jets continued to blow offshore with the Papagayo winds extending deep into the Pacific as an unbroken band of strong

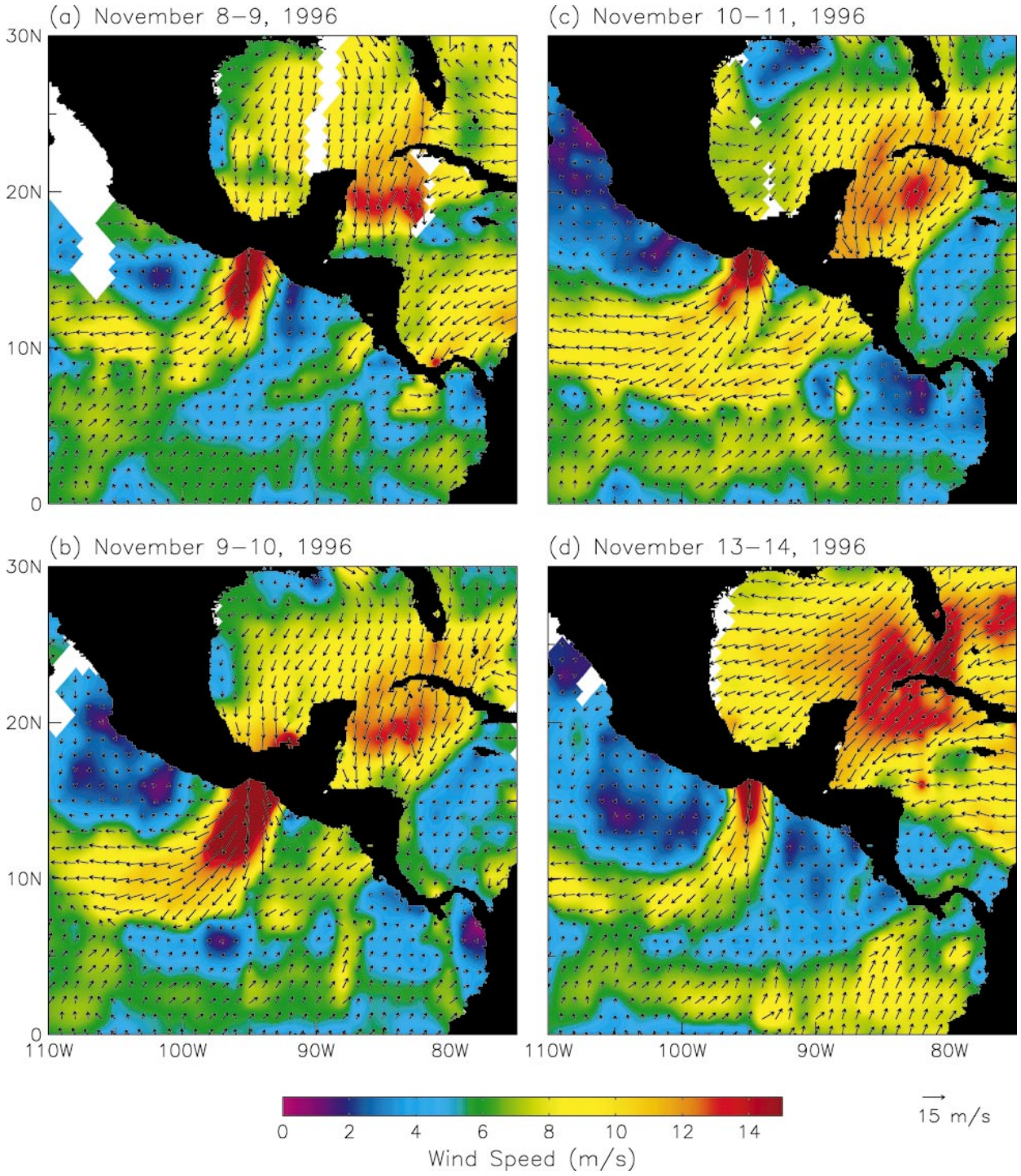

FIG. 7. Two-day composite maps of the wind field at 10 m from NSCAT data for the selected periods indicated during the November case study. The color bar is selected as described in the caption for Fig. 5.

northeasterly flow spanning the entire domain of interest and continuing to merge with the Pacific trade winds (Fig. 9c).

During 11–13 March, the north–south gradient of SLP between the southern United States and the Bay of Campeché was weak (Fig. 8d) and winds over the Gulf of Tehuantepec remained light (Fig. 9d). The winds over the Gulfs of Papagayo and Panama continued to blow under the influence of the Caribbean trade winds, but with somewhat decreased intensity and areal extent, ev-

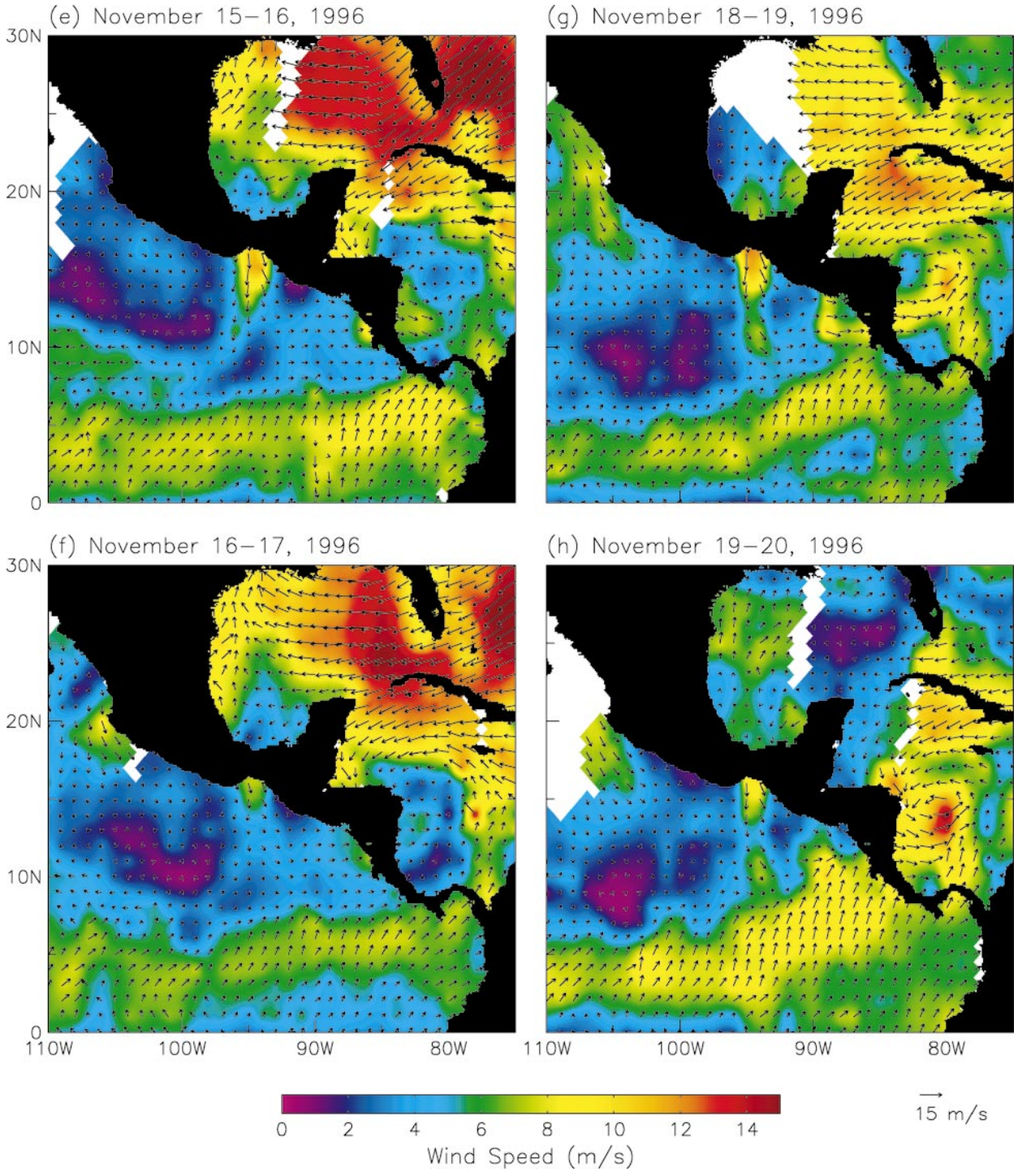

FIG. 7. (*Continued*)

idently in association with a weakening of the Caribbean trade winds (Fig. 9d).

The persistence of the Papagayo and Panama jets during this case study appears to be very similar to the 7–20 March 1985 case study described by Legeckis (1988). From persistent tongues of cold water in satellite observations of SST, he inferred that offshore winds blew persistently over the Gulfs of Papagayo and Panama. As in the March 1997 case study described here, the persistent Papagayo and Panama winds during the

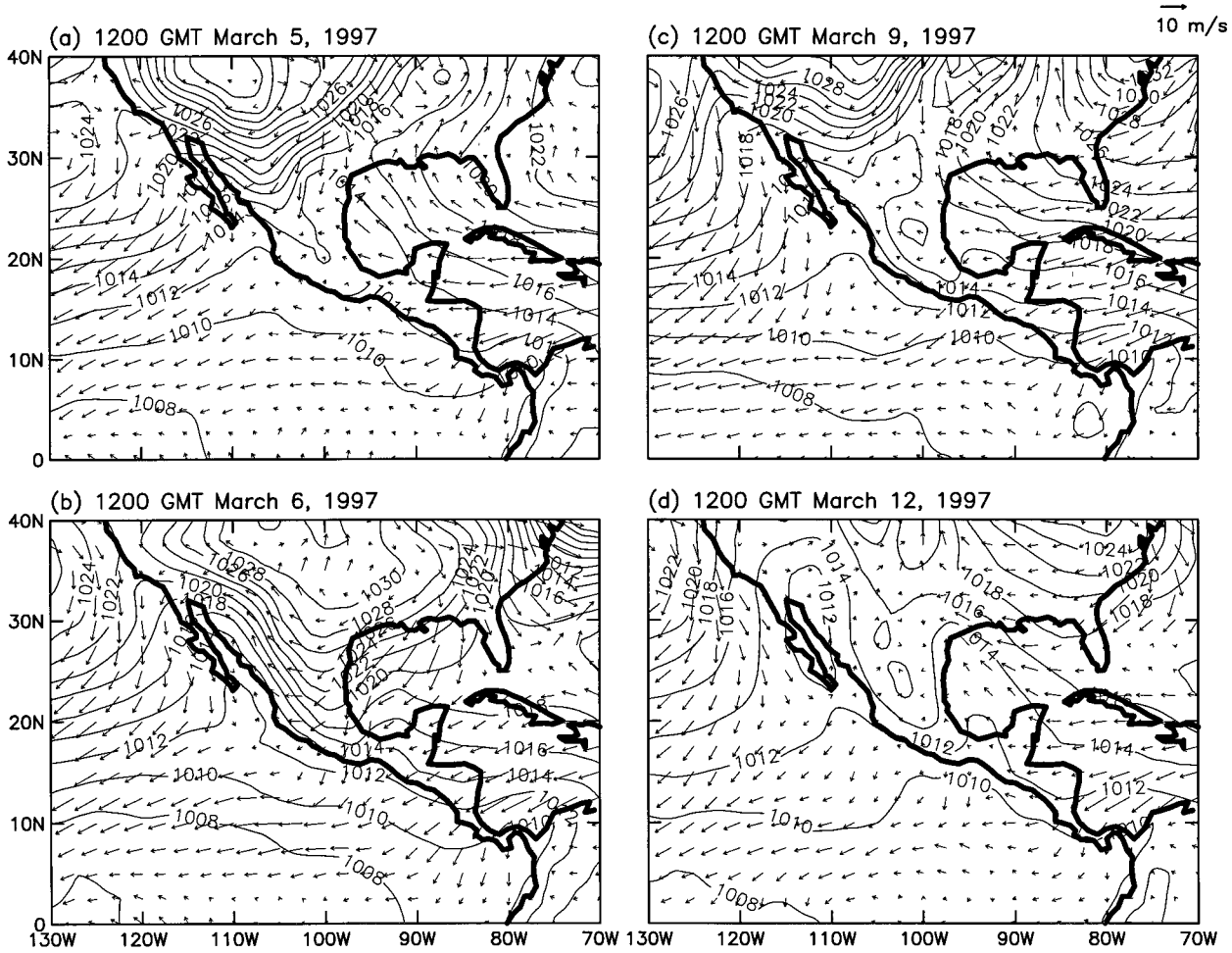

FIG. 8. Sea level pressure and 10-m winds from the 2.5°-gridded NCEP reanalyses for the selected times indicated during the Mar case study.

March 1985 case study investigated by Legeckis (1988) occurred during a period when winds over the Gulf of Tehuantepec were relatively weak.

4. Statistical characteristics of the three major wind jets

The characteristics of the Central American wind jets during the three time periods described in section 3 are representative of the wide diversity of conditions that existed over the 9-month duration of the NSCAT data record. The statistics of winds in this region are summarized in this section.

The temporal variability of the winds at near-coastal locations in the cores of the three jets during the full 9-month data record is shown by the vector time series in Fig. 10. The unique characteristics of the Tehuantepec jet are immediately apparent; the winds were much more variable and attained much higher speeds than the winds in either of the other two jets. From October through May, the Tehuantepec winds were predominantly offshore, with only a few periods of very weak onshore flow. There were no strong northerly winds over the Gulf of Tehuantepec during the last month of the NSCAT data record.

The Papagayo winds (middle panel of Fig. 10) alternated between strong onshore and strong offshore flow during the first 2 months of the data record. The offshore flow over the Gulf of Papagayo from late October to mid November coincided with a period of sustained strong offshore flow over the Gulf of Tehuantepec. From late November until March, the Papagayo winds were persistently offshore. Thereafter, there were occasional brief periods of onshore flow.

The winds over the Gulf of Panama (bottom panel of Fig. 10) were much weaker than the Tehuantepec and Papagayo winds. The meteorological conditions responsible for the offshore flow in the Tehuantepec and Papagayo jets during the 3-week period from late October to mid November evidently did not penetrate as far south as Panama. The influence of the late stages of the 1996 Central American summer monsoon season

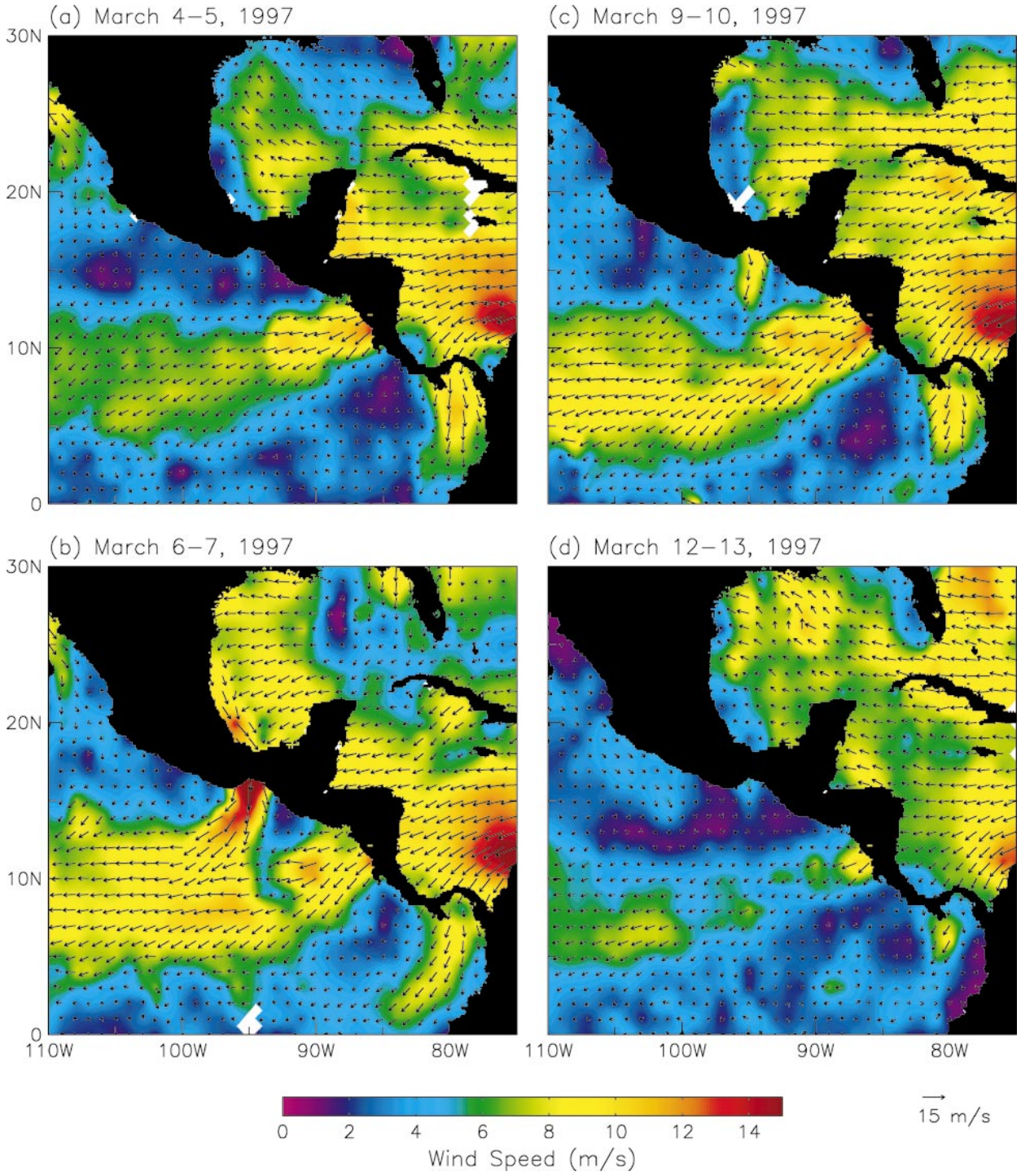

FIG. 9. Two-day composite maps of the wind field at 10 m from NSCAT data for the selected periods indicated during the Mar case study. The color bar is selected as described in the caption for Fig. 5.

(Mitchell and Wallace 1992) is evident from the persistent onshore flow throughout the first 2 months of the Panama data record. Except for brief periods of offshore winds in November, this seasonal monsoon influence continued until late November.

The seasonally persistent nature of southerly winds in Panama during September–November was first documented by Chapel (1927) from an analysis of 18 yr of wind observations at a coastal location on the west side of the Gulf of Panama. Chapel (1927) also pointed out

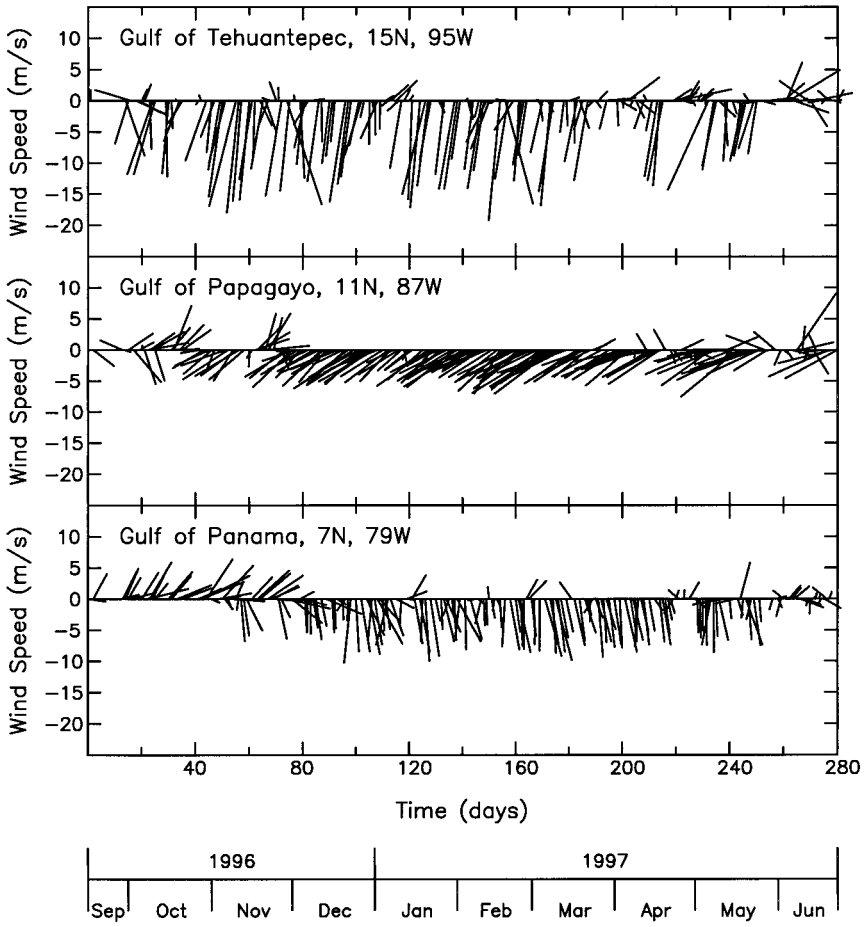

FIG. 10. Stick-plot time series of vector winds in the Gulf of Tehuantepec, the Gulf of Papagayo, the Gulf of Panama, and the Caribbean Sea. The latitudes and longitudes of the locations plotted are indicated in each panel. These locations correspond to the cores of the wind jets close to the coast.

that the southerly winds were associated with cross-equatorial flow in the eastern tropical Pacific. As noted in section 3b, Chapel (1927) also concluded that occasions when the southerly winds extend across the Isthmus of Panama into the Caribbean are almost always associated with the formation of cyclones in the western Caribbean.

It is evident from the Panama wind time series in the bottom panel of Fig. 10 that a transition from predominantly onshore monsoon flow to predominantly offshore flow occurred in early December 1996. From early December until late May, the winds over the Gulf of Panama were almost exclusively offshore, punctuated by occasional very brief episodes of weak onshore flow. This period of predominantly northerly winds coincides with the strong Caribbean trade winds that occur seasonally from November/December through April/May (Frankenfield 1917; Chapel 1927). The Panama wind speeds abruptly decreased in late May 1997 and became highly variable in direction throughout the month of June. From his analysis of 18 yr of coastal observations, Chapel (1927) found this to be a period of predominantly southerly winds in the Panama region. The normal southerly flow in June coincides with the beginning of the monsoon season when the region of maximum precipitation typically moves across the equator from South America into the Central American region (Mitchell and Wallace 1992). The abrupt decrease in the intensity of the Panama winds in late May and June during the NSCAT observational period thus presumably signaled the early stages of the 1997 transition to onshore monsoon winds.

For the purposes of this study, the 6-month period 1 December 1996–31 May 1997 during which the Panama winds were almost exclusively offshore will be defined to be the 1996–97 ''jet season.'' As also noted above, this coincides with the period of seasonally strong Caribbean trade winds (Frankenfield 1917; Chapel 1927). The statistical characteristics of the three individual jets are compiled in this section from the ensemble of wind events that occurred during this 6-month period.

The vector average, eddy kinetic energy, and velocity

variance ellipses (see Preisendorfer 1988) of the surface wind field measured by NSCAT during the 6-month jet season are shown in Fig. 11. In the Inter-American Seas, the mean wind field was dominated by the intense but very steady (small eddy kinetic energy) trade winds in the Caribbean Sea. The smallest vector average but most highly variable winds were found in the northern and western Gulf of Mexico. Over most of the Gulf of Mexico, the wind variability was only weakly anisotropic, as evidenced by the more nearly circular velocity variance ellipses than in the Pacific, for example (Fig. 11b). The most notable exception was the far western Bay of Campeché in which the velocity variance ellipses were highly anisotropic with major axes oriented approximately parallel to the steep topography of the Sierra Madre mountains.

In the Caribbean Sea, winds off the northwest coast of Colombia were highly anisotropic with major axes aligned parallel to the coastline. The winds were also anisotropic in the northwestern Caribbean with major axes aligned approximately east–west near Cuba and rotating counterclockwise to become approximately north–south over the Gulf of Honduras. The orientations of the major axes of variability were strongly influenced by orography close to the coast in the far western and southern Gulf of Honduras.

The most interesting features in the surface wind field were found on the Pacific side of Central America. The vector-average winds in Fig. 11a were dominated by the strong jets over the Gulfs of Tehuantepec, Papagayo, and Panama. Of the three jets, the mean winds were strongest in the Papagayo jet. The three jets also coincided with regions of large eddy kinetic energy in the eastern tropical Pacific. The variability of the Tehuantepec jet was the most energetic of the three jets and the variations of the Panama jet were the least energetic.

A noteworthy characteristic of all three jets is the ''fanning'' of the mean winds away from the axes of the jets. Similar fanning has been previously noted for the Tehuantepec jet by Barton et al. (1993) and Trasviña et al. (1995) from a 3-week composite average map of ship observations during a major wind event that occurred in January 1989. The fanning of the Tehuantepec jet has also been discussed by Steenburgh et al. (1998) from operational weather analyses and a mesoscale model simulation of an event that occurred in March 1993. The divergent flow along the axis of the jets associated with the fanning is investigated in detail by Chelton et al. (2000) for all three jets.

It is apparent from Fig. 11b that the velocity variance was highly anisotropic in all three jets. Over the Gulfs of Tehuantepec and Papagayo, the fluctuating winds were aligned approximately parallel to the mean wind vectors, indicating that the eddy kinetic energy was dominated by variations in the intensity, rather than the direction, of the winds in the jet regions. This implies consistencies in the orientations of fanning winds at each location from one wind event to another, despite

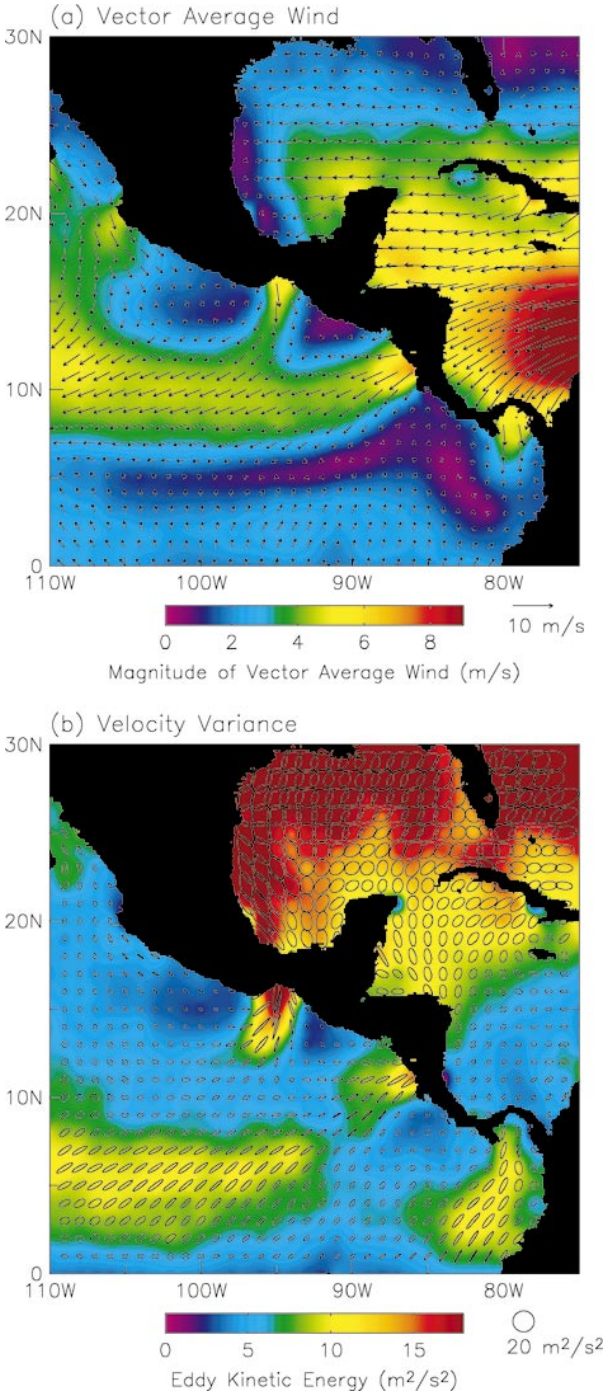

FIG. 11. Maps of NSCAT measurements of (a) the vector-average winds at 10 m, overlaid on a color map of the magnitude of the vector-average winds; and (b) the wind velocity variance ellipses for the same time period, overlaid on a color map of the eddy kinetic energy per unit mass. The means and variances were computed from all of the raw NSCAT observations in each 1° × 1° square during the 6-month jet season 1 Dec 1996–31 May 1997. The color table for each panel was selected to highlight the spatial structures of the Central American jets of interest in this study.

the wide ranges of the intensities of the winds (see also the narrow distributions of wind directions in Fig. 12). Over the Gulf of Panama, the major axes of the velocity variance ellipses were also approximately parallel to the mean vectors near the gap outflow. Farther offshore, however, the mean winds in the Panama jet became very weak while the orientations of the major axes of the velocity variance ellipses exhibited a well-defined clockwise rotation toward northeast-to-southwest orientation.

Between the three jets and to the west of the Tehuantepec jet, the weak vector-average winds in Fig. 11a and the small velocity variances in Fig. 11b indicate that the winds were persistently weak within about 200 km of the coastline. All three of these areas of light coastal winds are in the lee of tall mountain ranges (see Fig. 1). The northerly winds over the western Gulf of Mexico are funneled through Chivela Pass to form the Tehuantepec jet and the Caribbean trade winds are funneled through the low-altitude passes over the Nicaraguan lake district and the Panama Canal to form the Papagayo and Panama jets.

It is interesting to note from Fig. 11a that the mean surface winds are strong onshore along the entire western boundary of the Caribbean Sea. The mean outflows through the Papagayo and Panama gaps clearly cannot account for all of this onshore mean flow, suggesting that upward motion must take place over Central America to compensate for the apparent strong convergence in the surface wind field. This is consistent with the climatological pattern of higher wintertime cloudiness and precipitation on the Caribbean side of Central America (Hastenrath 1967; DeWitt et al. 1996).

At lower latitudes, a zonal band of locally strong northeast winds is evident in the mean wind field along 10°N, linking the Tehuantepec and Papagayo jets near the Central American coastline with the Pacific northeast trade winds. These downwind extensions of the Tehuantepec and Papagayo jets in the mean wind field can thus be interpreted as part of the Pacific northeast trade wind system.

A well-defined intertropical convergence zone (ITCZ) extended zonally along 5°N from the central Pacific to about 90°W, where it turned northeast to Costa Rica. A second convergence zone extended southeast from Costa Rica to the southern coast of Colombia, apparently from the convergence of the northerly winds over the Gulf of Panama and the southwesterly cross-equatorial flow. West of 90°W, the ITCZ region of small vector-average winds coincided with a region of high and very anisotropic variability; the fluctuating winds in this segment of the ITCZ were aligned from southwest to northeast, becoming much less variable outside of this band.

An especially interesting feature in the eastern tropical Pacific wind field was the band of persistent cross-equatorial mean surface flow across the entire domain of interest in Fig. 11a. From the coast of Ecuador to about 100°W, these cross-equatorial winds developed a distinct westerly component between about 1°N and 3°N. The small eddy kinetic energy equatorward of about 2°N (Fig. 11b) indicates the steady nature of this cross-equatorial flow. The orientations of the velocity variance ellipses indicate that those fluctuations that did exist were predominantly aligned with the vector-average winds. An analysis for different frequency bands reveals that the orientations of the fluctuations are essentially the same for the low-frequency (seasonal) variations as for the higher-frequency fluctuations. It is also noteworthy that this cross-equatorial flow was much stronger and extended farther west during the first 2 months of the NSCAT mission that have been excluded from the jet season statistics in Fig. 11.

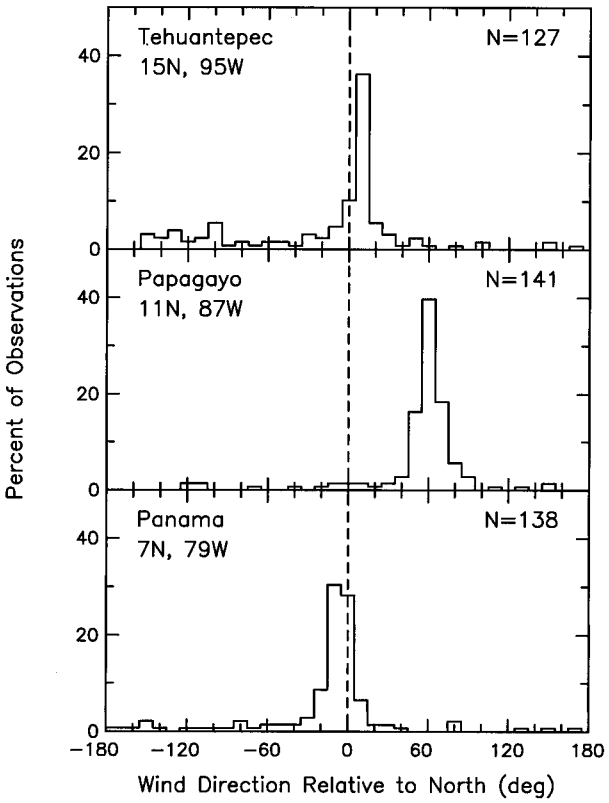

FIG. 12. Histograms of the meteorological wind directions (clockwise relative to north) in the vector wind time series shown in Fig. 10 during the 6-month jet season 1 Dec 1996–31 May 1997. The number of samples *N* from which the histogram was obtained is labeled at the upper-right corner of each panel.

The emphasis hereafter is on the characteristics of the three wind jets along the Pacific coast during the 6-month jet season December 1996–May 1997. A histogram of the directions of the Tehuantepec winds at 15°N, 95°W (about 100 km south of the coast) is shown in the top panel of Fig. 12. Over this 6-month period, 52% of the observations corresponded to winds with directions in the offshore range of 5° ± 15° clockwise relative to north. Over the same 6-month period, 75% of the observed Papagayo winds at 11°N, 87°W had

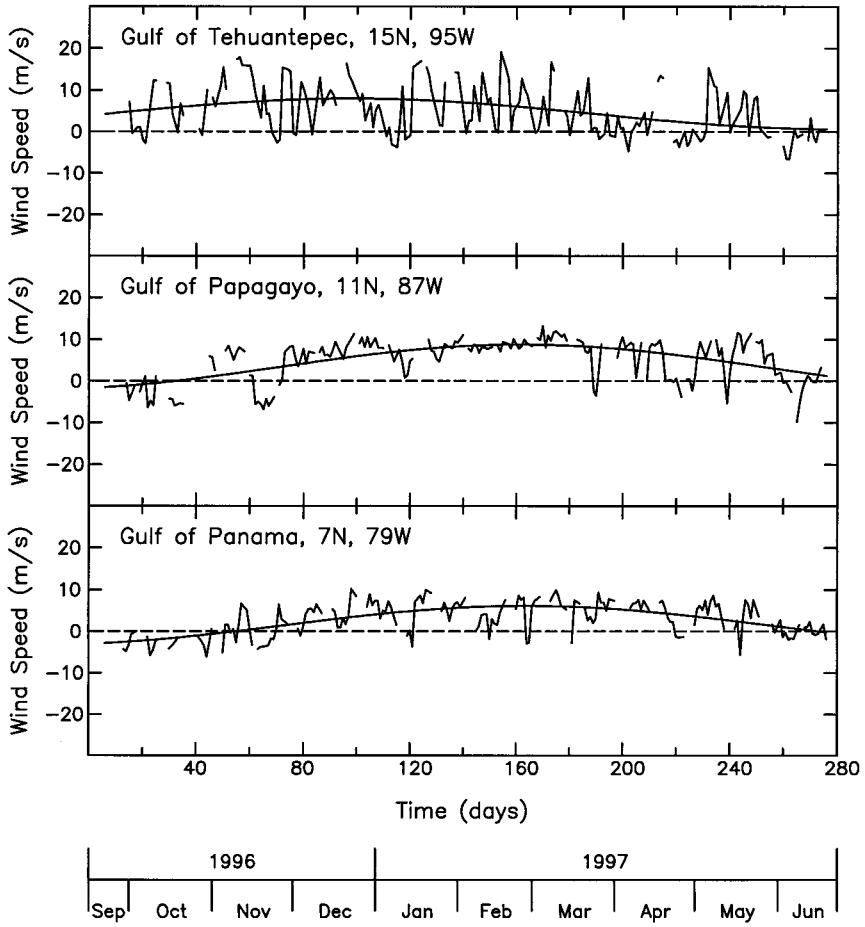

FIG. 13. Time series of the wind component along the major axis of the 6-month velocity variance ellipse in Fig. 11b at the location of each of the vector time series shown in Fig. 10. The smooth lines represent least-squares fits to annual and semiannual harmonics at each location. Sign convention is positive for offshore winds.

directions in the offshore range of 55° ± 15° (see middle panel of Fig. 12). The directional variability of the Panama winds at 7°N, 79°W was about midway between those of the Tehuantepec and Papagayo jets; 66% of the Panama observations during this 6-month period had directions in the offshore range of −10° ± 15° (see bottom panel of Fig. 12). The histograms in Fig. 12 thus show that the Papagayo jet was the most polarized of the three jets.

An important distinction between the winds at the three locations is a fundamental difference in the timescales of variability. The time series of the major-axis wind component in each jet (the component of the vector wind parallel to the major axis of the 6-month velocity variance ellipse) is shown in Fig. 13 and the corresponding autocorrelation functions for the full 9-month NSCAT data record are shown by the heavy lines in Fig. 14. The more persistent character of the Papagayo and Panama jets is evident from their longer autocorrelation timescales; the autocorrelation function decreases to a value of about 0.4, for example, at a lag of 2 days for Tehuantepec as compared with lags of about a week for Papagayo and 4 days for Panama.

It is apparent from Fig. 13 that there are underlying strong seasonal variations of the winds in the Papagayo and Panama jets. The smooth time series in Fig. 13 represent least-squares fits to the sum of annual and semiannual harmonies at each of the locations over the full 9-month duration of the NSCAT data record. The seasonal variation of the Papagayo and Panama jets accounts for 34% and 54% of the variances, respectively. The offshore flow in these jets was maximum during late February or early March. In contrast, the seasonal variation of the Tehuantepec jet, which accounts for only 16% of the variance, was maximum in December.

The phasing of the maximum winds in the Papagayo and Panama jets is almost identical to the seasonal cycle of winds in the Gulf of Panama region deduced by Chapel (1927) from 18 yr of wind observations at a coastal location on the west side of the gulf. He noted that the February maximum of Panama winds coincides with the seasonal maximum of the Caribbean trade winds.

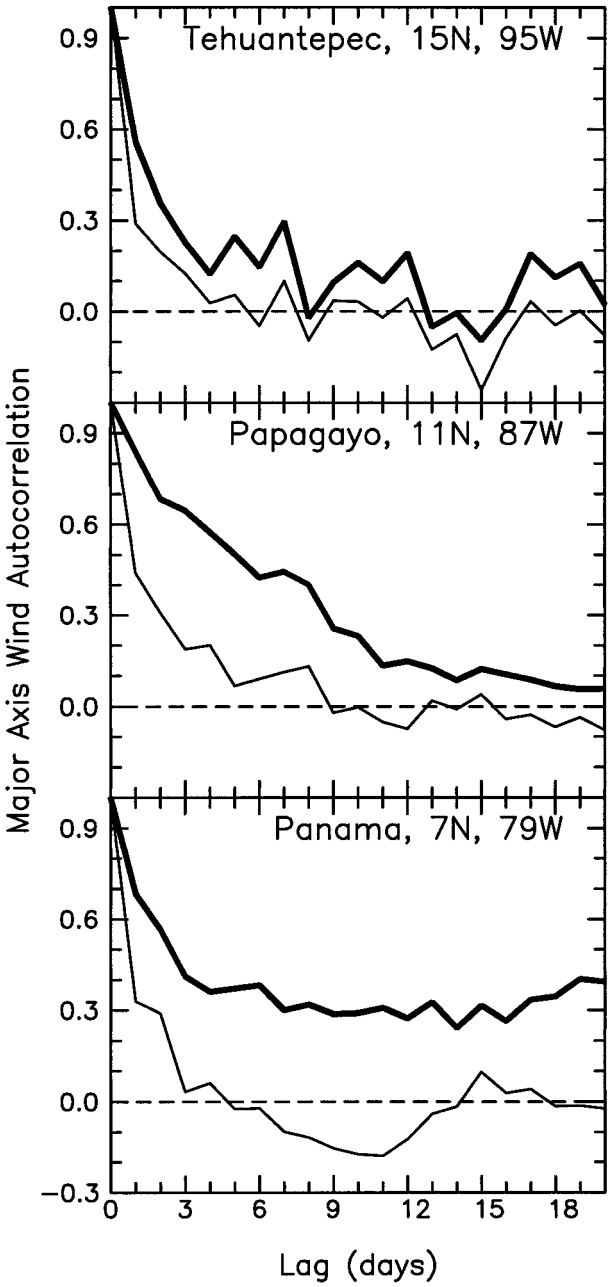

FIG. 14. Autocorrelation functions for the major-axis wind component time series shown in Fig. 13. The heavy lines correspond to the autocorrelation functions for the raw winds at each location over the full 9-month duration of the NSCAT data record. The thin lines correspond to the autocorrelation functions over just the 6-month jet season Dec 1996–May 1997 after removal of the low-frequency seasonal variations shown by the smooth lines in Fig. 13.

The seasonal variations of the Papagayo and Tehuantepec winds during the NSCAT observational period are also similar to the seasonal cycles of phytoplankton biomass presented by Lluch-Cota et al. (1997) for the Gulfs of Tehuantepec and Papagayo. Increased phytoplankton productivity is coupled to nutrients injected from the deep water into the surface layer from wind-induced mixing. Periods of high phytoplankton biomass would therefore be expected to occur during periods of strong winds. From 8 yr of satellite data, they found that phytoplankton biomasses in the Gulfs of Tehuantepec and Papagayo were maximum in December and April, respectively. From satellite observations along a transect along the west coast of South America, Fiedler (1994) similarly found that the seasonal maximum phytoplankton biomass occurred in early winter in the Gulf of Tehuantepec and in late winter/early spring in the Gulfs of Papagayo and Panama.

We thus conclude that the low-frequency variations of the winds in Fig. 13 are representative of the normal seasonal cycles of the three jets. The deviations of the raw winds from the seasonal variations represent ''events'' that are superimposed on the low-frequency seasonal variations. The thin lines in Fig. 14 correspond to the autocorrelation functions of these short-period (nonseasonal) variations during the 6-month jet season December 1996 through May 1997. In the Tehuantepec jet, the autocorrelation timescales of the nonseasonal variations are only slightly different from those of the raw winds. In contrast, removal of the seasonal variations results in significantly shorter autocorrelation timescales in the Papagayo and Panama jets, indicating that the persistence of the Papagayo and Panama jets is mostly attributable to the underlying seasonal variation. The event timescales in the Panama jet were approximately the same as the 2-day timescales of the Tehuantepec jet. In comparison, event timescales in the Papagayo jet were about 4 days.

Histograms of the major-axis wind component during the 6-month jet season December 1996–May 1997 are shown in Fig. 15. (As noted in section 2, the wind speeds in this analysis may be biased somewhat low since they were computed as daily averages over 1° square areas.) The dominance of offshore winds in the Papagayo jet is apparent from the middle panel; 92% of the Papagayo winds were offshore. The persistence of the Papagayo jet is evident from the fact that 52% of the observations had offshore speeds in the narrow range of 6–9 m s^{-1}. Only 5% of the Papagayo observations had wind speeds in excess of 10 m s^{-1}.

The dominance of offshore winds in the Panama jet during the 6-month jet season is also apparent; 86% of the winds were offshore and 40% of the observations had offshore speeds in the narrow range of 5–8 m s^{-1}. There was an abrupt decrease in the frequency of occurrence of winds with higher offshore speeds. The observed wind speeds never exceeded 10 m s^{-1}. The light winds observed over the Gulf of Panama during the NSCAT observational period are evidently typical of the winds in this region. From his analysis of 18 yr of wind observations at a coastal station on the west side of the Gulf of Panama, Chapel (1927) found that only 2% of the observed winds exceeded 10 m s^{-1}.

The offshore winds in the Tehuantepec jet were spread

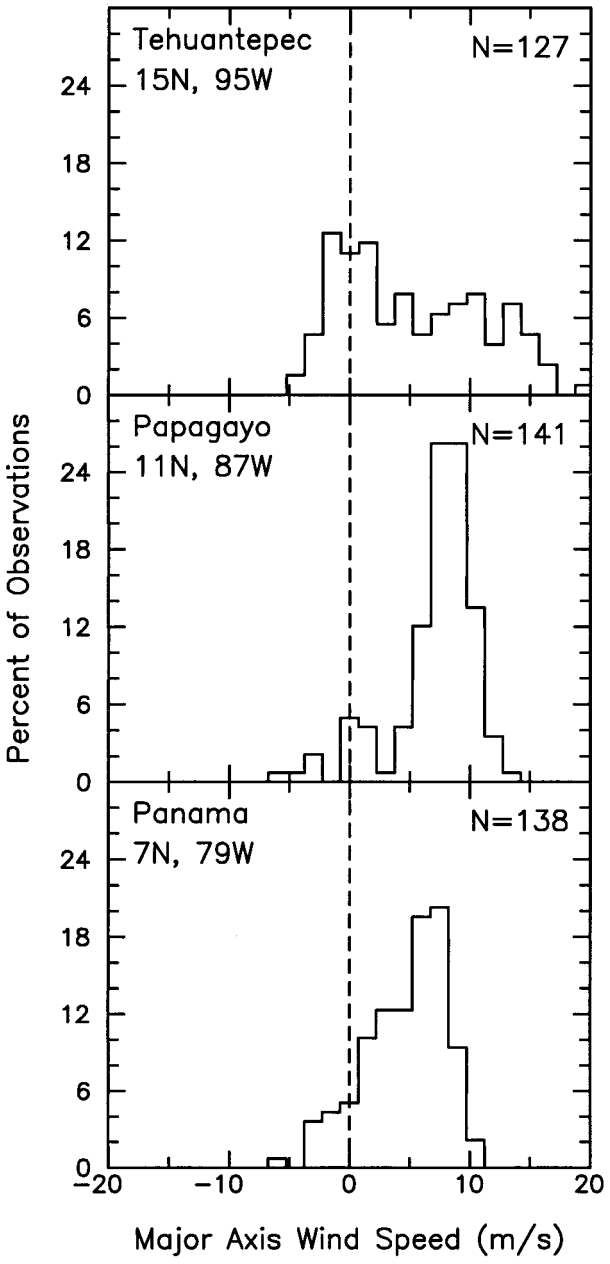

FIG. 15. Histograms of the major-axis wind component time series shown in Fig. 13 for the 6-month period 1 Dec 1996 through 31 May 1997. The number of samples *N* from which the histogram was obtained is labeled at the upper-right corner of each panel.

over a much broader continuum of speeds. This ''noisier'' character of the Tehuantepec histogram reflects the more sporadic nature of the Tehuantepec jet noted previously from the higher eddy kinetic energy and shorter timescales of variability of the Tehuantepec winds. During the 6-month jet season, 70% of the Tehuantepec winds were offshore. The distribution of offshore winds was roughly flat out to wind speeds of 13 m s^{-1}, above which the distribution tapered to zero at about 20 m s^{-1}. Overall, 20% of the observed wind speeds exceeded 10 m s^{-1} offshore, emphasizing the much more energetic character of the Tehuantepec jet.

5. Summary

Nine months of satellite microwave radar measurements by the NASA scatterometer (NSCAT) have provided the first observations of surface winds with accuracy, resolution, and coverage sufficient to describe the spatial characteristics and the statistics of the variability of surface winds in the three major wind jets along the Pacific coast of Central America. An animation of the complete 9-month NSCAT dataset in the Central America region of interest in this study can be viewed on the following web site: http://www.oce.orst.edu/po/research/windjets/movie.html. The 2-day composite averages over 1° × 1° areas in these maps of the wind fields are the most nearly synoptic measurements presently available for investigation of these jets. Although sampling errors are a concern with averaging periods this short, the 2-day composite averages provide new insight into the statistical characteristics of the winds in this region.

The three Central American wind jets were examined from detailed analyses of case studies and from the statistical properties of winds near the coast in the three individual jets. The three case studies presented in section 3 were specifically selected from more than a dozen major Tehuantepec wind events in order to illustrate the wide diversity of relationships that exist between the three jets.

In all three case studies, the Tehuantepec jet developed immediately after the appearance of high sea level pressure in the Gulf of Mexico. The Papagayo and Panama jets were sequentially triggered after the onset of major Tehuantepec events during the December case study in section 3a and during the early stages of the November case study in section 3b. However, the intensities of the Papagayo and Panama jets varied independently of the Tehuantepec jet during the late stages of the November case study and throughout the period of the March case study in section 3c.

The lack of synchrony between the Tehuantepec jet and the two lower-latitude jets in the March case study described here appears to be very similar to a March 1985 case study described by Legeckis (1988). Likewise, the influence of tropical storm Marco on the Papagayo and Panama jets in the November case study appears to be typical of conditions during the formation of cyclones in the western Caribbean (Chapel 1927). Evidently more than one mechanism can affect the Papagayo and Panama jets.

The distinction between the Tehuantepec jet and the Papagayo and Panama jets is further underscored by the statistical characteristics presented in section 4. To maximize the temporal resolution, the averaging period for the 1° × 1° averages was reduced to 1 day for the

purposes of these statistical analyses. In addition to having much larger maximum wind speeds, the Tehuantepec jet was also much more transient than the other two jets. About one-third of the variability in the Papagayo jet and one-half of the variability in the Panama jet consisted of low-frequency seasonal variations. These two lower latitude jets were thus much more persistent than the Tehuantepec jet for which seasonal variability accounted for only about one-sixth of the variance. Superimposed on the seasonal variations, there were events with timescales in the Panama jet that were comparable to the 2-day timescales in the Tehuantepec jet. Event timescales in the Papagayo jet were about double those of the Tehuantepec and Panama jets.

The analyses presented here are the most complete observational description of the surface wind field yet available for this region. While there is no doubt that the sequential north-to-south triggering of these jets by high pressure systems of midlatitude origin that penetrate as far south as the southern Caribbean Sea plays a role in the development of some wind events (see, e.g., Schultz et al. 1997), it is clear from two of the three case studies in section 3 that the Papagayo and Panama jets are sometimes strongly influenced by trade wind fluctuations and other tropical phenomena that have little or no effect on the Tehuantepec jet. The much greater persistence of the Papagayo and Panama jets (the longer autocorrelation timescales in Fig. 14 and the stronger seasonal variability in Fig. 13) is further evidence of the fundamentally different character of these two lower-latitude jets. It is therefore highly unlikely that the midlatitude high pressure systems that sweep from northwest to southeast across the Inter-American Seas are the primary factor affecting the variability of the Papagayo and Panama jets. It is much more likely that variations of these two lower-latitude jets are coupled to variations in the Caribbean trade winds that are funneled through the Papagayo and Panama gaps.

Schultz et al. (1997, 1998) have recently suggested that variations of the Caribbean trade winds are associated with midlatitude cyclones that originate over the Great Plains of North America, move southeastward across the Gulf of Mexico, and settle over the western Atlantic. By this scenario, there could be an indirect link between the cold surges that drive the Tehuantepec jet and the trade wind mechanism proposed here for the generation of Papagayo and Panama jets. However, the dynamics of the trade wind mechanism are fundamentally different from the across-gap pressure difference that generates the Tehuantepec jet. Thus, while the synoptic-scale disturbances that generate Tehuantepec wind events may also modify the trade wind flow, thereby generating Papagayo and Panama winds, this is very different from sequential north-to-south triggering of the gap winds by across-gap pressure differences associated with frontal passages sweeping southeastward across the Inter-American Seas. There is also the important point noted above that the timescales of jet variations are much longer in the Papagayo and Panama jets than in the Tehuantepec jet. If they are responsible for variability of the Papagayo and Panama jets, the high pressure systems associated with the Tehuantepec events must undergo major transformations of time- and space scales.

The relative importance of midlatitude versus tropical forcing of the gap outflows is investigated quantitatively in the companion paper to this study (Chelton et al. 2000). The speculation about the difference between the midlatitude anticyclone mechanism for the generation of the Tehuantepec jets and the trade wind mechanism for the generation of Papagayo and Panama jets is confirmed from statistical relationships between the three jets and large-scale surface wind and pressure fields. The companion paper also investigates dynamical balances within the three jets.

Acknowledgments. We thank Michael Schlax for preparing the figures and for many helpful discussions and suggestions that greatly improved the manuscript, Dean Vickers for help with the NCEP sea level pressure and 10-m wind fields presented in section 3, Michael Caruso and Kathie Kelly for providing the collocated NSCAT/TAO data analyzed in section c of the appendix, and David Long for providing the raw NSCAT cell location data used to construct Fig. A2. We also thank David Schultz and an anonymous reviewer for their careful reading of the manuscript and constructive suggestions for improvement. The research presented in this paper was supported by Contracts 957580 and 959351 from the Jet Propulsion Laboratory funded under the NSCAT Announcement of Opportunity and NOAA Grants NA56GP0208 and NA76GP0404 from the Office of Global Programs.

APPENDIX

Radar Scatterometry

Scatterometers are spaceborne radars designed to measure near-surface vector winds over the ocean. The scatterometer measurement technique is indirect and empirical models are used for some critical aspects of the technique. The principles of scatterometry are briefly summarized in this appendix.

a. NSCAT overview

Spaceborne microwave scatterometers measure the normalized radar cross section (σ_0) of the earth's surface by transmitting pulses of microwave radiation and measuring the magnitude of the backscattered energy. The NSCAT instrument used eight fan-beam antennas to acquire multiple σ_0 measurements within a pair of 600-km swaths separated by a 329-km gap centered on the satellite ground track (Fig. A1). The principal scattering mechanism at microwave frequencies and moderate in-

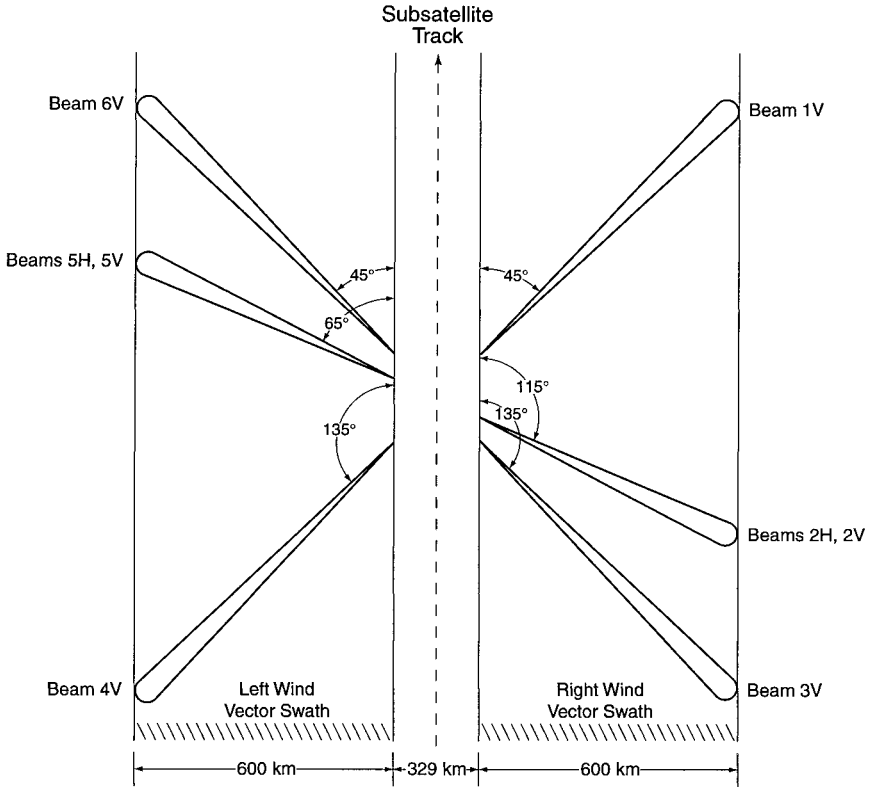

FIG. A1. Schematic plan view of the NSCAT vector wind swaths and principal antenna pointing directions (after Naderi et al. 1991).

cidence angles is resonant (''Bragg'') scattering from short ocean waves that have length scales commensurate with the projection of the radar wavelength onto the sea surface. At the NSCAT frequency of 13.995 GHz, the ocean scattering elements have wavelengths ranging from ~1.2 cm at the 16° incidence angle at the inner edge of the NSCAT swaths to ~3.9 cm at the 65° incidence angle at the outer edge of the swaths. Except in moderate-to-heavy rainfall, the atmosphere is relatively transparent at scatterometer radar frequencies. The scatterometer is therefore a near all-weather instrument for measuring radar backscatter from the ocean.

Although the detailed physics underlying both radar scattering and wind wave generation are not completely understood, there is a strong empirical correlation between σ_0 and wind velocity. The nature of this empirical relation is summarized by Naderi et al. (1991) and the references therein. At incidence angles from about 15° to 65°, σ_0 increases with increasing wind speed and varies approximately as $\cos(2\chi)$, where the relative azimuth χ is the horizontal angle between the incident radar direction and the wind direction. For a given wind speed and incidence angle, σ_0 is largest at upwind ($\chi = 0°$) and downwind ($\chi = 180°$) azimuths (when the radar direction is roughly perpendicular to the crests and troughs of wind-generated centimetric waves), and smallest at cross-wind angles. The upwind–crosswind σ_0 ratio increases with increasing incidence angle and is largest at low wind speeds.

In addition to the primary upwind–crosswind modulation, there is a small difference between upwind and downwind σ_0 values for incidence angles exceeding about 20° (slightly greater upwind than downwind). Although in principle the upwind–downwind asymmetry allows determination of a unique wind direction based on scatterometer σ_0 measurements alone, the small magnitude of the asymmetry, measurement noise, and uncertainties in the precise relationship between σ_0 and vector wind pose operational challenges that limit the ability to determine wind direction as summarized in section b of this appendix.

The surface vector wind can be estimated by combining temporally and spatially collocated σ_0 measurements acquired from different azimuths, polarizations, and incidence angles. The nominal pointing angles for NSCAT are shown in Fig. A1. Vertically polarized backscatter measurements were taken at each of the three antenna pointing angles, while a fourth antenna acquired horizontally polarized data at the midbeam angles. Each location on the earth's surface was illuminated sequentially by the fore, mid, and aft antennas. For the ~6.7 km s^{-1} ground track speed of the spacecraft, the time difference between fore and aft beam measurements at

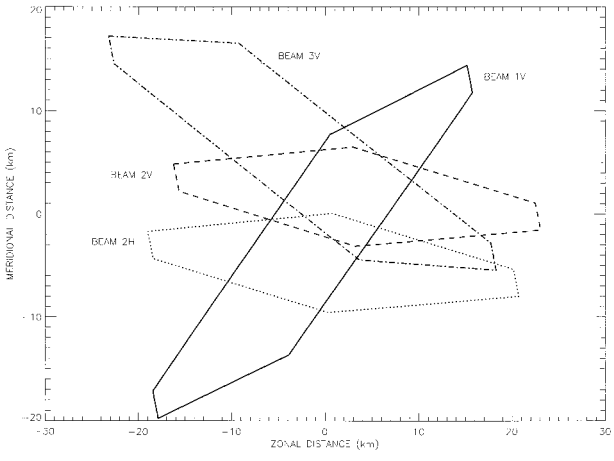

FIG. A2. Collocated 25-km NSCAT σ_0 cells from a near-equatorial, midswath location.

the same point on the ocean varied from ~30 s in the near swath to ~230 s at far swath.

The instantaneous illumination pattern of the NSCAT fan beam antennas consisted of elongated areas spanning the full width of the measurement swath (see Fig. A1). The backscattered radar signal is Doppler shifted by the relative motion of the orbiting satellite and the rotating earth. This Doppler shift increases with increasing incidence angle, thus allowing a specific electromagnetic frequency to be associated with a specific point on the sea surface along the fan beam of the antenna. The Doppler-shifted returned signal from each antenna beam was Fourier transformed onboard the spacecraft and σ_0 was calculated in each of 24 variable-width frequency bands allowing 25-km along-beam spatial resolution (Naderi et al. 1991). The along-track width of the σ_0 cells was defined by the 0.4° bandwidth of the fan-beam antennas and the 0.486-s dwell time during which each antenna was sequentially activated. A full cycle of all eight antennas was completed every 3.73 s, during which the spacecraft moved 25 km. Individual NSCAT σ_0 cells thus had characteristic dimensions of 6 km × 25 km. The set of cells with collocated centroids from all four antennas on one side of the spacecraft illuminated a unique area of about $(25 \text{ km})^2$ on the sea surface (Fig. A2). Automatic calibration cycles, during which no σ_0 measurements were taken, occurred every 128 antenna cycles (~8 min). As vector winds were retrieved only when valid σ_0 measurements were available from each of the four antennas, these calibration cycles result in periodic data gaps resembling the antenna beam patterns in Fig. A1 (see, e.g., Fig. 2).

b. Wind retrieval and ambiguity removal

The NSCAT winds analyzed in this study were estimated using the empirical NSCAT-1 model function (Wentz and Smith 1999; Freilich and Dunbar 1999, unpublished manuscript) and a maximum likelihood retrieval algorithm (Naderi et al. 1991, and references therein) that relate vector winds to σ_0 and the radar frequency, polarization, and incidence angle. The approximate $\cos(2\chi)$ dependence of σ_0, coupled with the NSCAT fan-beam geometry and noise in the σ_0 measurements, resulted in up to four potential vector wind solutions at each swath location. The solutions (referred to as ''ambiguities'') had similar wind speeds but widely different directions. The retrieval algorithm yielded an estimate of the probability that each ambiguity was the ''correct'' solution, based on the mismatch between the measured and predicted values of σ_0.

For the NSCAT-1 dataset, a unique vector wind was selected at each measurement location using a circular median filter algorithm that eliminated short-scale directional variability while preserving wind field features such as fronts that had significant length scales in at least one dimension (Naderi et al. 1991, and references therein). Following initialization, the filter was applied iteratively until convergence. For each iteration and measurement location, the selected wind velocity was that of the ambiguity closest to the median direction within the filter region, without regard to the probability value calculated during wind retrieval.

The median filter must be initialized with a trial wind direction at each measurement location. Prelaunch simulations indicated that the two ambiguities with the largest probabilities were usually very close to 180° apart, were oriented approximately parallel to the surface vector wind, and had similar probability magnitudes. Thus, although the NSCAT measurement geometry had extremely high skill in identifying the wind ''streamline,'' the small upwind–downwind asymmetry in σ_0 for a given wind speed often resulted in the most probable ambiguity differing from the true wind direction by approximately 180°. The median filter therefore could not be accurately initialized by simply using only the highest probability ambiguity. The limited numerical-weather-prediction-aided initialization approach described by Freilich (1994) was therefore employed for the NSCAT processing. This scheme makes use both of the inherent skill in the scatterometer measurements and additional information from operational surface wind analyses. At each location, the initial direction was chosen to be that of either the most probable or the second-most-probable ambiguity, depending on which was closest in direction to the contemporaneous 2.5°-gridded NCEP operational surface analysis.

It is important to emphasize that the NSCAT wind retrievals were not rigidly constrained to match the wind directions in the operational analyses. The iterative ambiguity removal processing often resulted in the selection of ambiguities that were orthogonal or even opposite to the wind directions in the operational analyses. Moreover, owing to spatial coherences in the NSCAT solution patterns and the inherent information content of the NSCAT measurements, the locations of synoptic features in the final NSCAT unique vector wind dataset

were often significantly displaced from those in the operational NCEP prediction used to initialize the median filter algorithm. Case study analyses and comparisons with independent information have shown that such discrepancies are generally attributable to errors in the operational analyses (Brown and Zeng 1994; Atlas et al. 1999).

The circular medians were calculated over a 175-km square area centered on each NSCAT measurement location within the swath. The filter nominally covered 49 wind vector cells, but fewer measurements were available near the swath edges, coasts, and in regions of missing NSCAT data. In addition, the information content in both the NSCAT ambiguities and the NCEP operational analyses was low in regions of low wind speed (<3 m s^{-1}). The global validation analysis by Freilich and Dunbar (1999) indicates that only a few percent of the NSCAT vector wind directions were contaminated by large ambiguity removal errors. The circular median filter algorithm can, of course, result in more frequent errors in the vicinity of geographically isolated wind patterns.

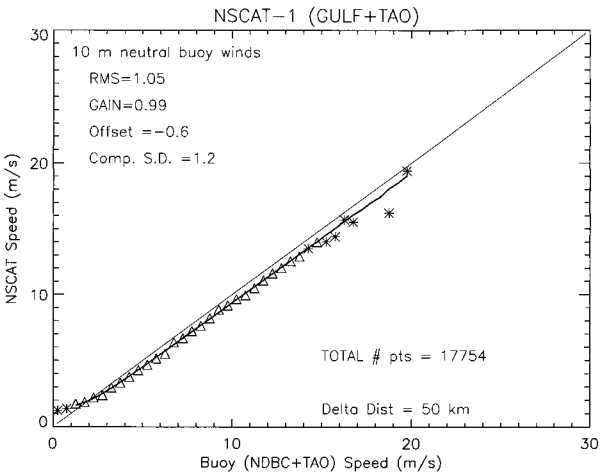

FIG. A3. Wind speed comparisons between 17 754 collocated NSCAT and buoy measurements from the Gulf of Mexico (NDBC) and eastern tropical Pacific (TAO). Each point displayed in the plot represents the mean value of the NSCAT wind speeds for the corresponding 0.5 m s^{-1} buoy wind speed bin. Triangles (asterisks) denote binned mean values calculated from more (fewer) than 100 collocations. The heavy solid line corresponds to the best-fit nonlinear regression curve, including the effects of component error standard deviation, computed by the method developed by Freilich (1997).

c. Vector wind accuracy

Comprehensive validations of NSCAT estimates of vector winds have been reported by Freilich and Dunbar (1999) and Freilich and Vanhoff (2000, submitted to *J. Atmos. Oceanic Technol.*) based on comparisons with midlatitude National Data Buoy Center (NDBC) operational meteorological buoys. A regional validation for the Central American region of interest here was performed using only comparisons with 16 NDBC buoys in the Gulf of Mexico and 7 Tropical Ocean–Atmosphere (TAO) buoys spanning latitudes 0°–8°N at 110° and 95°W (McPhaden et al. 1998). Collocation cutoff radii of 30 min and 50 km were used, and buoy anemometer measurements were converted to equivalent 10-m neutral-stability winds using the boundary layer transformation of Liu and Tang (1996) and auxiliary meteorological variables measured by the buoys. There were significant (>100 day) gaps in several of the TAO buoy records. A total of 17 754 collocations with NDBC and TAO buoy observations were obtained, of which about 10% were from TAO buoys.

Using the method developed by Freilich (1997) and applied to the full midlatitude NDBC buoy dataset by Freilich and Dunbar (1999), comparison of NSCAT speeds with the regional buoy data resulted in a mean offset of -0.6 m s^{-1} (NSCAT low with respect to the buoys) and a root-mean-square (rms) difference of 1.1 m s^{-1} (Fig. A3). After elimination of data contaminated by ambiguity removal errors (assumed to be the cause of directional differences exceeding $\pm 90°$; see Freilich and Dunbar 1999), the standard deviation of directional differences over the range 3–20 m s^{-1} was $\sim 19°$. These regional buoy comparisons are quantitatively consistent with the rms speed difference of 1.2 m s^{-1} and rms direction difference of 17° obtained by Freilich and Dunbar (1999) from analysis of the complete midlatitude NDBC dataset. Ambiguity removal skill (as measured by direction difference magnitudes smaller than 90°) was 93.5% from the regional buoy comparison, which is consistent with the value of $\sim 97\%$ obtained for the full midlatitude NDBC buoy comparison.

It should be noted that not all of the rms difference between the NSCAT and buoy winds is due to errors in the NSCAT measurements. Buoy winds have been shown to have rms wind speed and direction errors of about 0.8 m s^{-1} and 10°, respectively (Gilhousen 1987; Beardsley et al. 1997; Freilich and Vanhoff 2000, submitted to *J. Atmos. Oceanic Technol.*). Assuming that the errors in the NSCAT and buoy measurements are independent, the partitioning of the rms differences as the root sum of squares of the separate measurement errors leads to the conclusion that the NSCAT measurement accuracy is very similar to that of the buoys.

REFERENCES

Atlas, R., S. C. Bloom, R. N. Hoffman, E. Brin, J. Ardizone, J. Terry, D. Bungato, and J. C. Jusem, 1999: Geophysical validation of NSCAT winds using atmospheric data and analyses. *J. Geophys. Res.*, **104,** 11 405–11 424.

Barton, E. D., and Coauthors, 1993: Supersquirt: Dynamics of the Gulf of Tehuantepec, Mexico. *Oceanography*, **6,** 23–30.

Beardsley, R. C., A. G. Enriquez, C. A. Friehe, and C. A. Alessi, 1997: Intercomparison of aircraft and buoy measurements of wind and wind stress during SMILE. *J. Atmos. Oceanic Technol.*, **14,** 969–977.

Bourassa, M. A., L. Zamudio, and J. J. O'Brien, 1999: Noninertial flow in NSCAT observations of Tehuantepec winds. *J. Geophys. Res.*, **104,** 11 311–11 319.

Brown, R. A., and L. Zeng, 1994: Estimating central pressures of oceanic midlatitude cyclones. *J. Appl. Meteor.,* **33,** 1088–1095.

Chapel, L. T., 1927: Winds and storms on the Isthmus of Panama. *Mon. Wea. Rev.,* **55,** 519–530.

Chelton, D. B., M. H. Freilich, and S. K. Esbensen, 2000: Satellite observations of Central American coastal wind jets. Part II: Regional relationships and dynamical considerations. *Mon. Wea. Rev.,* **128,** 2019–2043.

Clarke, A. J., 1988: Inertial wind path and sea surface temperature patterns near the Gulf of Tehuantepec and Gulf of Papagayo. *J. Geophys. Res.,* **93,** 15 491–15 501.

Colle, B. A., and C. F. Mass, 1995: The structure and evolution of cold surges east of the Rocky Mountains. *Mon. Wea. Rev.,* **123,** 2577–2610.

DeWitt, D. G., E. K. Schneider, and A. D. Vernekar, 1996: Factors maintaining the zonally asymmetric precipitation distribution and low-level flow in the Tropics of an atmospheric general circulation model: Diagnostic studies. *J. Atmos. Sci.,* **53,** 2247–2263.

Färber-Lorda, J., M. F. Lavin, M. A. Zapatero, and J. M. Robles, 1994: Distribution and abundance of euphausiids in the Gulf of Tehuantepec during wind forcing. *Deep-Sea Res.,* **41,** 359–367.

Fiedler, P. C., 1994: Seasonal and interannual variability of coastal zone color scanner phytoplankton pigments and winds in the eastern tropical Pacific. *J. Geophys. Res.,* **99,** 18 371–18 384.

Frankenfield, H. C., 1917: ''Northers'' of the Canal Zone. *Mon. Wea. Rev.,* **45,** 546–550.

Freilich, M. H., 1994: ERS-1 scatterometer measurements over the Southern Ocean. *Proc. Second ERS-1 Symp.,* Hamburg, Germany, ESA, 1111–1115.

——, 1997: Validation of vector magnitude data sets: Effects of random component errors. *J. Atmos. Oceanic Technol.,* **14,** 695–703.

——, and R. S. Dunbar, 1999: The accuracy of the NSCAT-1 vector winds: Comparisons with National Data Buoy Center buoys. *J. Geophys. Res.,* **104,** 11 231–11 246.

Gilhousen, D. B., 1987: A field evaluation of NDBC moored buoy winds. *J. Atmos. Oceanic Technol.,* **4,** 94–104.

Hastenrath, S. L., 1967: Rainfall distribution and regime in Central America. *Arch. Meteor. Geophys. Biokl., Series B,* **15,** 201–241.

Hurd, W. E., 1929: Northers of the Gulf of Tehuantepec. *Mon. Wea. Rev.,* **57,** 192–194.

Kalnay, E., and Coauthors, 1996: The NCEP–NCAR 40-Year Reanalysis Project. *Bull. Amer. Meteor. Soc.,* **77,** 437–471.

Legeckis, R. V., 1988: Upwelling off the Gulfs of Panama and Papagayo in the tropical Pacific during March 1985. *J. Geophys. Res.,* **93,** 15 485–15 489.

Liu, W. T., and W. Tang, 1996: Equivalent neutral wind. JPL Pub. 96-17, 8 pp. plus appendix. [Available from Jet Propulsion Laboratory, 4800 Oak Grove Drive, Pasadena, CA 91109.]

Lluch-Cota, S. E., S. Alverez-Borrego, E. M. Santamaria del Angel, F. E. Müller-Karger, and S. Hernández-Vázquez, 1997: The Gulf of Tehuantepec and adjacent areas: Spatial and temporal variation of satellite-derived photosynthetic pigments. *Ciencias Marinas,* **23,** 329–340.

McCreary, J. P., H. S. Lee, and D. B. Enfield, 1989: The response of the coastal ocean to strong offshore winds: With application to circulation in the Gulfs of Tehuantepec and Papagayo. *J. Mar. Res.,* **47,** 81–109.

McPhaden, M. J., and Coauthors, 1998: The Tropical Ocean–Global Atmosphere observing system: A decade of progress. *J. Geophys. Res.,* **103,** 14 169–14 240.

Mitchell, T. P., and J. M. Wallace, 1992: The annual cycle in equatorial convection and sea surface temperature. *J. Climate,* **5,** 1140–1156.

Naderi, F. M., M. H. Freilich, and D. G. Long, 1991: Spaceborne radar measurement of wind velocity over the ocean—An overview of the NSCAT scatterometer system. *Proc. IEEE,* **97,** 850–866.

Parmenter, F. C., 1970: A ''tehuantepecer.'' *Mon. Wea. Rev.,* **98,** 479.

Preisendorfer, R. W., 1988: *Principal Component Analysis in Meteorology and Oceanography.* Elsevier, 425 pp.

Schultz, D. M., W. E. Bracken, L. F. Bosart, G. J. Hakim, M. A. Bedrick, M. J. Dickinson, and K. R. Tyle, 1997: The 1993 Superstorm cold surge: Frontal structure, gap flow and tropical impact. *Mon. Wea. Rev.,* **125,** 5–39; Corrigenda, **125,** 662.

——, ——, and ——, 1998: Planetary- and synoptic-scale signatures associated with Central American cold surges. *Mon. Wea. Rev.,* **126,** 5–27.

Steenburgh, W. J., D. M. Schultz, and B. A. Colle, 1998: The structure and evolution of gap outflow over the Gulf of Tehuantepec, Mexico. *Mon. Wea. Rev.,* **126,** 2673–2691.

Stumpf, H. G., 1975: Satellite detection of upwelling in the Gulf of Tehuantepec, Mexico. *J. Phys. Oceanogr.,* **5,** 383–388.

Trasviña, A., E. D. Barton, J. Brown, H. S. Velez, P. M. Kosro, and R. L. Smith, 1995: Offshore wind forcing in the Gulf of Tehuantepec, Mexico: The asymmetric circulation. *J. Geophys. Res.,* **100,** 20 649–20 663.

Wentz, F. J., and D. K. Smith, 1999: A model function for the ocean normalized cross section at 14 GHz derived from NSCAT observations. *J. Geophys. Res.,* **104,** 11 499–11 514.